

N78-20076

NASA CR-145322  
CR-

**A CRITICAL EVALUATION OF THE PREDICTIONS OF THE  
NASA-LOCKHEED MULTIELEMENT AIRFOIL COMPUTER PROGRAM**

**Final Report**

**G. W. Brune and J. W. Manke**

**March 1978**

Prepared under contract **NAS1-14522** by  
**Boeing Commercial Airplane Company**  
P.O. Box 3707  
Seattle, Washington 98124

for  
**NASA-Langley Research Center**  
**National Aeronautics and Space Administration**



1. Report No. NASA CR-145322	2. Government Accession No.	3. Recipient's Catalog No.	
4. Title and Subtitle A CRITICAL EVALUATION OF THE PREDICTIONS OF THE NASA-LOCKHEED MULTIELEMENT AIRFOIL COMPUTER PROGRAM		5. Report Date March 1978	6. Performing Organization Code
		8. Performing Organization Report No. D6-45100	10. Work Unit No.
7. Author(s) G. W. Brune and J. W. Manke		11. Contract or Grant No. NAS1-14522	13. Type of Report and Period Covered Final-July 1976 to Jan. 1978
9. Performing Organization Name and Address Boeing Commercial Airplane Company P.O. Box 3707 Seattle, Washington 98124		14. Sponsoring Agency Code	
		12. Sponsoring Agency Name and Address Langley Research Center National Aeronautics and Space Administration Washington, D.C. 20546	
15. Supplementary Notes Technical Monitor, Dr. R. W. Barnwell NASA Langley Research Center Hampton, VA 23669			
16. Abstract Theoretical predictions of several versions of the NASA-Lockheed multielement airfoil computer program are evaluated. The computed results are compared with experimental high lift data of general aviation airfoils with a single trailing edge flap, and of airfoils with a leading-edge flap and double slotted trailing-edge flaps. Theoretical and experimental data include lift, pitching moment, profile drag and surface pressure distributions, boundary layer integral parameters, skin friction coefficients, and velocity profiles.			
17. Key Words (Suggested by Author(s)) Multielement airfoil Lift Pitching moment Profile drag		18. Distribution Statement Surface pressure Boundary layer Test theory comparison Unlimited - Unclassified	
19. Security Classif. (of this report) Unclassified	20. Security Classif. (of this page) Unclassified	21. No. of Pages 62	22. Price*

**Page intentionally left blank**

**Page intentionally left blank**

# CONTENTS

	Page
SUMMARY .....	1
INTRODUCTION .....	1
Program Versions .....	2
Baseline Version .....	2
Version A .....	2
Version B .....	2
Version C .....	2
Test Cases .....	3
ACKNOWLEDGEMENT .....	3
SYMBOLS .....	9
Abbreviations .....	10
EVALUATION OF PROGRAM PREDICTIONS .....	11
Single Airfoil .....	11
Basic GA(W)-1 Airfoil .....	11
Flat Plate .....	11
Two-Element Airfoils .....	18
GA(W)-1 With 30% Chord Flap .....	18
Foster's Airfoil .....	36
Ljungström's Airfoil .....	36
Four-Element Airfoils .....	36
Boeing High Lift Airfoil .....	36
Ljungström's Airfoil .....	54
CONCLUSIONS .....	60
REFERENCES .....	61

## FIGURES

No.	Page
1. Analyzed Airfoil Configurations .....	4
2. Geometry Definitions .....	8
3. Lift and Pitching Moment of GA(W)-1 Single Airfoil .....	12
4. Drag Polar of GA(W)-1 Single Airfoil .....	13
5. Surface Pressures of GA(W)-1 Single Airfoil .....	14
6. Flat Plate Wake Characteristics .....	16
7. Lift and Pitching Moment Characteristics of GA(W)-1 With 30% Chord Flap .....	19
8. Lift Curves of GA(W)-1 With 30% Chord Flap .....	20
9. Pitching Moment Characteristics of GA(W)-1 With 30% Chord Flap .....	21
10. Surface Pressure of GA(W)-1 With 30% Chord Flap .....	22
11. Drag Polar of GA(W)-1 With 30% Chord Flap .....	23
12. Surface Pressure of GA(W)-1 With 30% Chord Flap .....	25
13. Boundary Layer Thickness on Main Component of GA(W)-1 With 30% Chord Flap .....	28
14. Lift Curves of GA(W)-1 With 30% Chord Flap .....	29
15. Surface Pressure of GA(W)-1 With 30% Chord Flap .....	30
16. Skin Friction on Upper Surface of GA(W)-1 With 30% Chord Flap .....	31
17. Separation on Flap Upper Surface of the GA(W)-1 With 30% Chord Flap .....	32
18. Variation of Displacement Thickness During Iteration of Version A for GA(W)-1 .....	33
19. Boundary Layer Profiles, Comparison of Theory and Experiment for GA(W)-1 With 30% Chord Flap, $\alpha = 2.7^\circ$ , $\delta_F = 40^\circ$ .....	34
20. Pressure Distribution on Flap for Foster Two-Element Airfoil .....	35
21. Boundary Layer Parameters on Flap Upper Surface of Foster Two-Element Airfoil .....	37
22. Lift and Drag Comparison for Ljungström Two-Element Airfoil .....	38
23. Lift Curve of Boeing Four-Element Airfoil .....	39
24. Drag Polar of Boeing Four-Element Airfoil .....	40
25. Drag of Boeing Four-Element Airfoil .....	41
26. Pitching Moment Characteristics of Boeing Four-Element Airfoil .....	43
27. Convergence Characteristics of Program Versions for Boeing Four-Element Airfoil .....	44
28. Slat Surface Pressures of Boeing Four-Element Airfoil .....	45
29. Pressure Distribution Comparison for Main Wing Section of Boeing Four-Element High-Lift Airfoil .....	47
30. Wing Surface Pressures of Boeing Four-Element Airfoil .....	48
31. Pressure Distribution Comparison for Main Flap of Boeing Four-Element High-Lift Airfoil .....	49
32. Main Flap Surface Pressures of Boeing Four-Element Airfoil .....	50
33. Trailing-Edge Flap Pressures of Boeing Four-Element Airfoil .....	51
34. Computed Position of Wake Centerlines of Boeing Four-Element Airfoil .....	52

35.	Boundary Layer Displacement Thickness on Upper Surface of Main Wing of Boeing Four-Element Airfoil .....	53
36.	Viscous Flow on Upper Surface of Boeing Four-Element High-Lift Airfoil, $\alpha = 8.4^\circ$ , $M_\infty = 0.16$ , $R_N = 2 \times 10^6$ .....	55
37.	Computed Boundary Layer Thickness on Upper Surface of Boeing Four-Element Airfoil .....	56
38.	Boundary Layer Profiles on Upper Wing Surface of Boeing Four-Element Airfoil .....	57
39.	Boundary Layer Profiles of Boeing Four-Element High-Lift Airfoil .....	58
40.	Comparison of Lift- and Drag-Coefficient for Ljungström Four-Element Airfoil .....	59

## SUMMARY

The theoretical predictions of several versions of the NASA-Lockheed multielement airfoil computer program are evaluated. The computed results are compared with experimental high lift data of general aviation airfoils with a single trailing edge flap, and of airfoils with a leading edge flap and double slotted trailing edge flaps. Detailed test-theory comparisons are reported for the GA(W)-1 with a 30% chord flap and a Boeing four-element high-lift airfoil. Theoretical and experimental data comprise global airfoil parameters such as lift, pitching moment, and profile drag, as well as surface pressure distributions, boundary layer integral parameters, skin friction coefficients, and velocity profiles. The evaluated versions of the computer program include the *baseline version* that was available from NASA in June 1976, and three versions that were developed by The Boeing Company in a joint NASA-Boeing effort. The results of this evaluation show that the contract objectives of improving program reliability and accuracy have been met.

## INTRODUCTION

This document reports on an evaluation of the predictions of several versions of the NASA-Lockheed computer program for two-dimensional multielement airfoils. The original version was developed by Goradia and his coworkers at Lockheed Georgia under the sponsorship of the NASA-Langley Research Center (ref. 1). The program was later modified extensively in order to improve its predictions for the different types of high-lift airfoils. Many improvements, mainly in the area of the potential flow calculation, were made by researchers at the Langley Research Center (ref. 2). Recently, members of the Aerodynamic Research Group of the Boeing Commercial Airplane Company supported by numerical analysts of Boeing Computer Services (BCS) substantially modified the aerodynamic model, its numerical implementation, and the computer code.

This work, reported in two engineering documents (refs. 3 and 4) and in this supplemental document, was sponsored jointly by NASA and The Boeing Company. In particular, the evaluation of the computer program by comparison with recent experimental high-lift data was a joint NASA-Boeing effort.

The objective of the evaluation was to learn as much as possible about the range of applicability and the deficiencies of the aerodynamic model. For that reason those sets of experimental data were preferred and investigated in detail which not only offered global aerodynamic force and moment coefficients but also information on pressure distributions and boundary layer parameters.

It should be emphasized that the test theory comparison reported in this document is by no means complete or exhaustive. However, enough information has been accumulated during the evaluation period to justify the publication of a separate document. Revisions of the document will be made later as new versions of the computer program and additional experimental data become available.

## PROGRAM VERSIONS

The following defines the various versions of the computer program emphasizing their differences.

### BASELINE VERSION

This version was supplied to Boeing by NASA-Langley prior to the beginning of the contract work. A description is not available but most aspects of its underlying aerodynamic theory are discussed in references 1 and 2. The main assumptions of the aerodynamic model are:

- Flow is two-dimensional and subcritical
- Flow is attached to the airfoil's surface
- High-lift airfoil consists of up to four components
- Geometry of the high-lift airfoil is discretized by up to 165 surface points

### VERSION A

This is the baseline version of the code made operational for airfoils with negative overlap of neighboring components.

### VERSION B

This version is thoroughly documented in reference 3. The following areas differentiate version B from the baseline version.

- The prediction method of Nash for ordinary turbulent boundary layer flow is replaced by the method of Nash and Hicks (ref. 5).
- The drag prediction method of Squire and Young (ref. 6) replaces the previous pressure and skin friction integration.
- Several logical errors in the baseline version are corrected.

### VERSION C

The following describes the differences between the aerodynamic theory and the Version B theory of the NASA-Lockheed program (ref. 4).

- The method used to represent the displacement effect of viscous layers is replaced by the surface transpiration method. This uses an equivalent distribution of sources along the airfoil surface and along the wake centerlines.

- The flow model of the region containing a potential core is modified. Wake properties are calculated using the lag entrainment method of Green (ref. 7) and transition from laminar to turbulent boundary layer flow may take place in the core region.
- By using a modified version of Goradia's confluent boundary layer model an attempt is made to predict the onset of separation of confluent boundary layers. The modification utilizes Coles' two-parameter velocity profile for the wall layer (ref. 8).
- The high-lift airfoil may consist of up to 10 airfoil components.
- The computer code of this version uses a dynamic storage allocation thereby removing the limitation on the number of geometry points representing airfoil surfaces.

### TEST CASES

The geometries of all airfoil configurations that were used for the evaluation are shown in figure 1. Geometric details of these airfoils such as flap settings, gap, and overlap of airfoil components are listed in tables 1, 2, and 3. Furthermore these tables contain the flight condition, i.e., angle of attack, Mach number, and Reynolds number, at which the test theory comparisons were conducted. Figure 2 illustrates the definitions of the most important geometry parameters.

### ACKNOWLEDGEMENT

Versions A and B of the program were evaluated by Dr. Mansop Hahn of the Boeing Commercial Airplane Company.

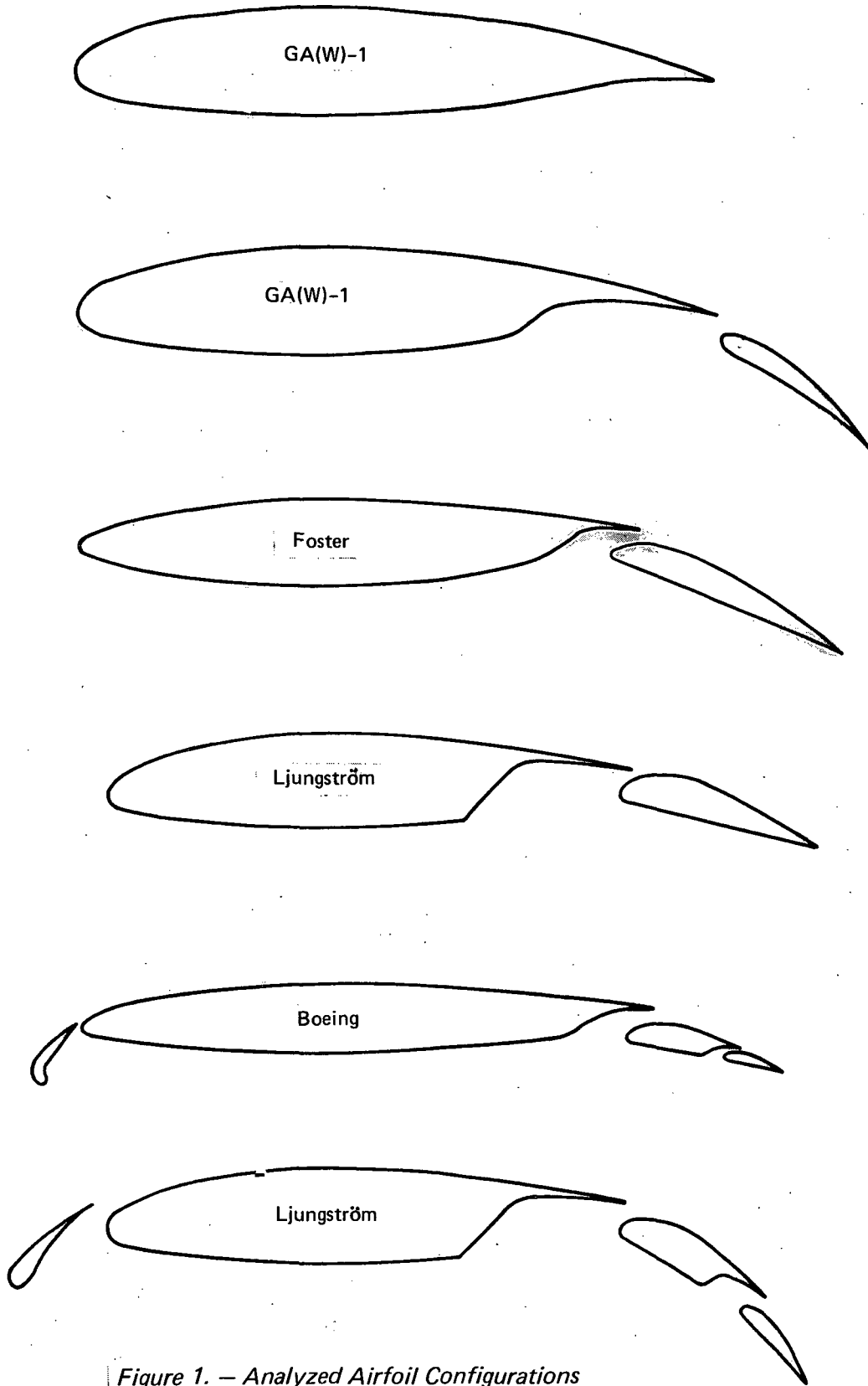
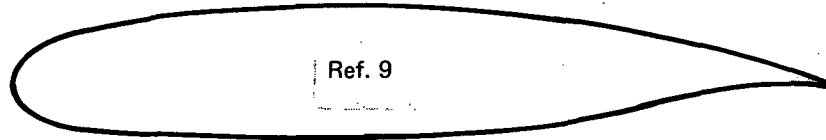


Figure 1. — Analyzed Airfoil Configurations

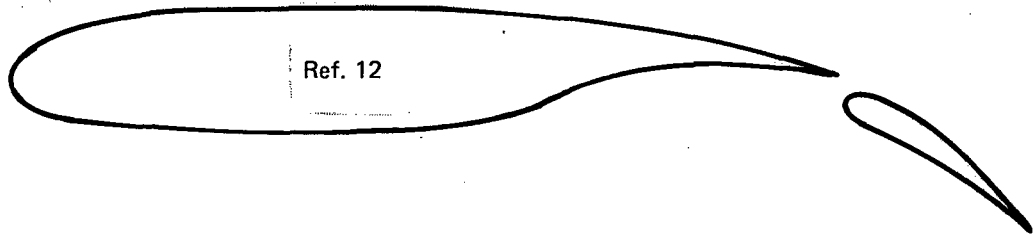
Table 1. — GA (W)-1 Airfoil Cases

(a) GA (W)-1 Basic Airfoil,  $c_{ref} = 1.917$  ft



$\alpha = -4.11^\circ, 0^\circ, 4.17^\circ, 8.02^\circ, 12.04^\circ$   
 $M_\infty = 0.15$   
 $R_N = 6.3 \times 10^6$

(b) GA(W)-1 With 30% Chord Trailing-Edge Flap,  $c_{ref} = 2$  ft

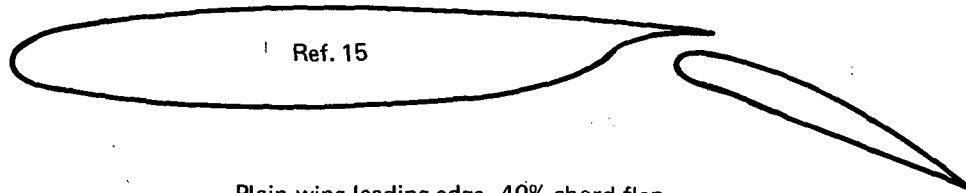


$\delta F$ degree	Gap % chord	Overlap % chord	$\alpha$ degree
10	2.5	7.1	-4.0, 0.2, 5.2, 10.3, 12.8
20	2.5	4.7	0.2, 5.2, 10.3, 12.8
30	2.5	2.1	-4.0, 0.1, 5.2, 10.3, 12.8
40	2.6	-0.85	2.7

$M_\infty = 0.13$   
 $R_N = 2.2 \times 10^6$

Table 2. — Additional Two-Element Airfoil Cases

(a) Foster's Two-Element Airfoil,  $c_{ref} = 3$  ft



Plain wing leading edge, 40% chord flap

$\delta_F$	=	$30^\circ$	Gap	2.5% chord
$M_\infty$	=	0.18 (?)	Overlap	4.3% chord
$R_N$	=	$3.6 \times 10^6$ (?)		
$\alpha$	=	$0^\circ$		

(b) Ljungström's Two-Element Airfoil,  $c_{ref} = 2.133$  ft

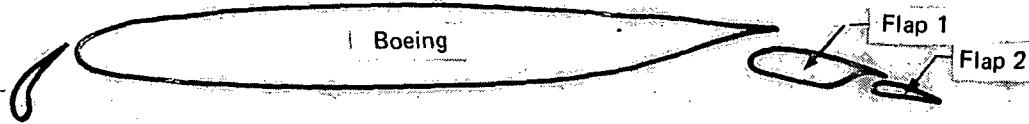


Configuration 1                      32% chord flap

$\delta_F$	=	$20^\circ$	Gap	2% chord
$M_\infty$	=	0.12	Overlap	1.54% chord
$R_N$	=	$1.83 \times 10^6$		
$\alpha$	=	$0^\circ$		

Table 3. – Four-Element Airfoils

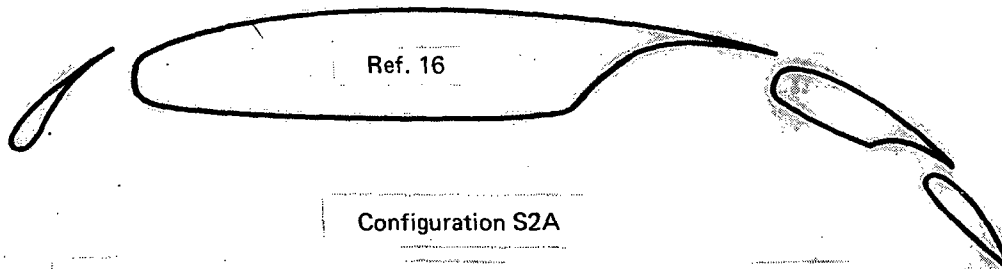
(a) Boeing Airfoil,  $c_{ref} = 2$  ft



Slat			Flap 1			Flap 2		
$\delta_s$	Gap % $c_{ref}$	Chord % $c_{ref}$	$\delta_F$	Gap % $c_{ref}$	Chord % $c_{ref}$	$\delta_F$	Gap % $c_{ref}$	Chord % $c_{ref}$
53°	1.4	11.2	11°	2.8	19.4	13°	0.5	9.9

$M_\infty = 0.16$   
 $R_N = 2 \times 10^6$   
 $\alpha = 4.4^\circ, 8.4^\circ, 12.45^\circ, 16.6^\circ, 20.6^\circ$

(b) Ljungström Four-Element Airfoil,  $c_{ref} = 2.133$  ft



Configuration S2A

Slat			Flap 1			Flap 2		
$\delta_s$	Gap % $c_{ref}$	Chord % $c_{ref}$	$\delta_F$	Gap % $c_{ref}$	Chord % $c_{ref}$	$\delta_F$	Gap % $c_{ref}$	Chord % $c_{ref}$
20°	4.0	18.5	35°	3.1	25.1	55°	2.5	16

$M_\infty = 0.12$   
 $R_N = 1.83 \times 10^6$   
 $\alpha = 10^\circ, 16^\circ$

top

5.5/8" x 8 5/8" IMAGE AREA

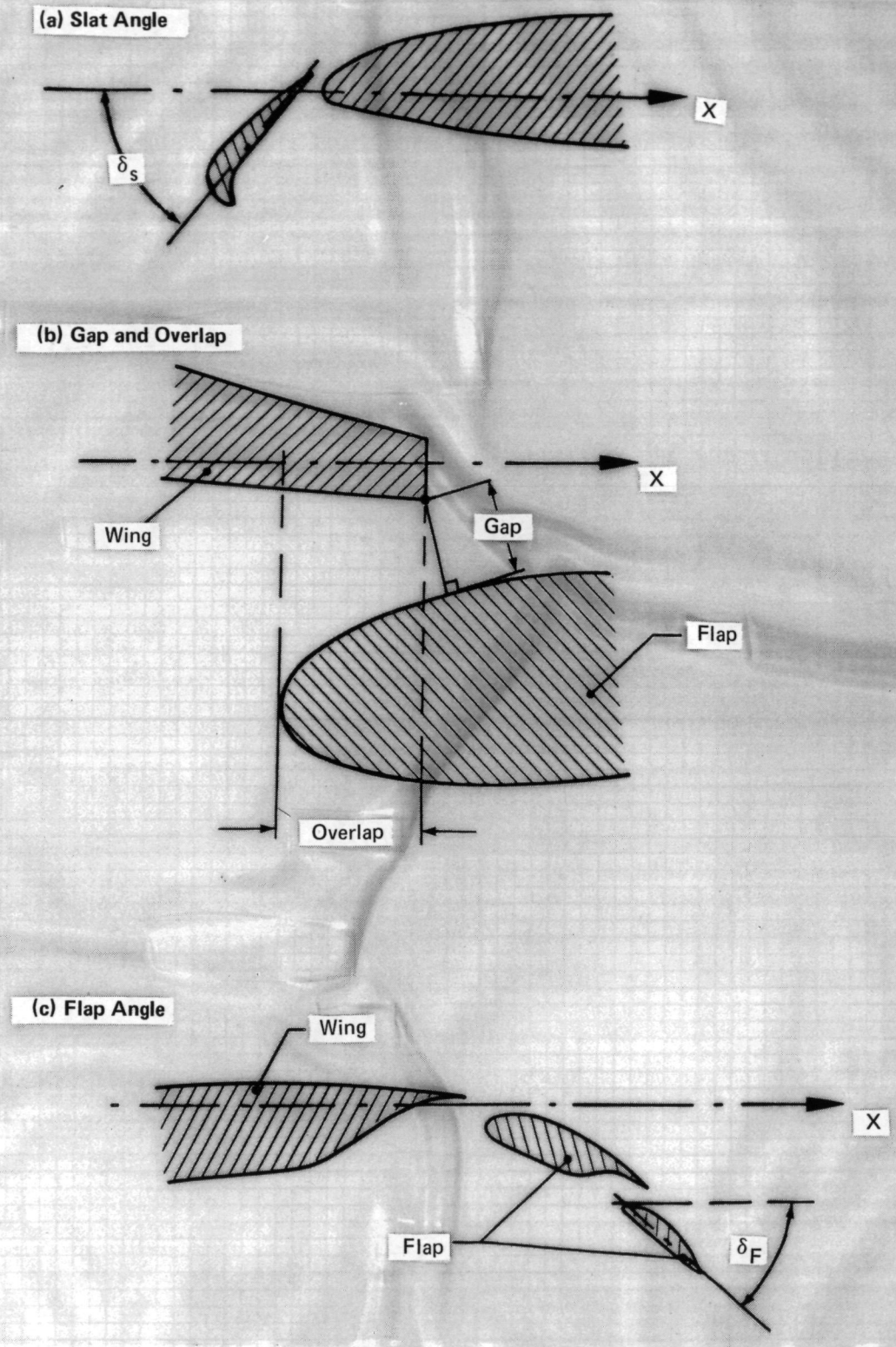


Figure 2. — Geometry Definitions

## SYMBOLS

Symbol	Definition
$C_d$	coefficient of profile drag
$C_f$	skin friction coefficient
$C_L$	lift coefficient
$C_m$	pitching moment coefficient about the quarter chord point
$C_p$	surface pressure coefficient
$C_{ref}$	wing reference chord in feet
$M_\infty$	freestream Mach number
$Re_N = U_\infty C_{ref} / \nu$	Reynolds number formed by freestream velocity and wing reference chord
$U_\infty$	freestream velocity
$u$	velocity component tangential to airfoil surface
$X$	X-coordinate of axis system of main airfoil component
$X_F$	X-coordinate of flap axis system
$Y$	coordinate measured perpendicular to airfoil surface
$Z$	Z-coordinate of axis system of main airfoil
$\alpha$	angle of attack in degrees
$\delta_F$	flap angle
$\delta_l$	boundary layer thickness on lower surface
$\delta_s$	slat angle
$\delta^*$	boundary layer displacement thickness
$\delta$	boundary layer or wake thickness
$\theta$	boundary layer or wake momentum thickness
$\delta_u$	boundary layer thickness on upper surface

## ABBREVIATIONS

FT fixed transition

LS laminar short bubble

S separation

T transition

## EVALUATION OF PROGRAM PREDICTIONS

The comparisons of theoretical and experimental high-lift data are discussed in the same order in which the analyzed airfoil configurations are listed in figure 1 and tables 1, 2, and 3.

### SINGLE AIRFOIL

#### BASIC GA(W)-1 AIRFOIL

The basic GA(W)-1 airfoil was chosen to test the program capability of predicting performance characteristics of single airfoils. Figures 3 and 4 contain theoretical lift, pitching moment, and drag curves and their comparison with experimental data of McGhee and Beasley (ref. 9). Both Version A and the new Version C programs predict identical lift and moment curves that in turn agree well with measured GA(W)-1 data up to the onset of trailing edge stall at about  $8^\circ$  angle of attack.

Considerable differences between all drag polars are observed in figure 4. Version A, utilizing an integration of surface pressure and skin friction in the prediction of profile drag, gives the highest drag coefficients. Version C, applying the Squire and Young formula, offers drag values that are lower than the corresponding experimental drag coefficients. The lack of agreement of the three drag polars emphasizes the fact that even for single airfoils at low speed the problem of obtaining accurate drag computations is not yet solved.

Surface pressures of the GA(W)-1, computed by program Version C and plotted in figure 5 at two different angles of attack, agree reasonably well with their experimental counterpart. At the lower angle of attack the flow is attached to the entire airfoil surface; whereas, at the higher angle of attack a laminar short bubble with subsequent turbulent reattachment of the boundary layer is indicated near the upper surface leading edge, and turbulent boundary layer separation is predicted theoretically near the upper surface trailing edge. The latter prediction is confirmed by the experimental pressure distribution which shows a constant pressure downstream of the theoretical point of separation.

In all figures of this document, the arrows and the symbols S and LS refer to theoretical points of turbulent separation and laminar short bubbles, respectively. The symbol FT indicates the experimental trip strip location which is specified as a fixed transition point in the computer simulation. The symbol T denotes a computed free transition point.

#### FLAT PLATE

Figure 6 shows a test theory comparison of a different kind that was used to judge the quality of the wake flow calculations of Green's lag entrainment method (ref. 7). The experimental data of the wake behind a flat plate at zero angle of attack were taken from test case 14 of the NASA-Langley Conference on Free Turbulent Shear Flows (refs.

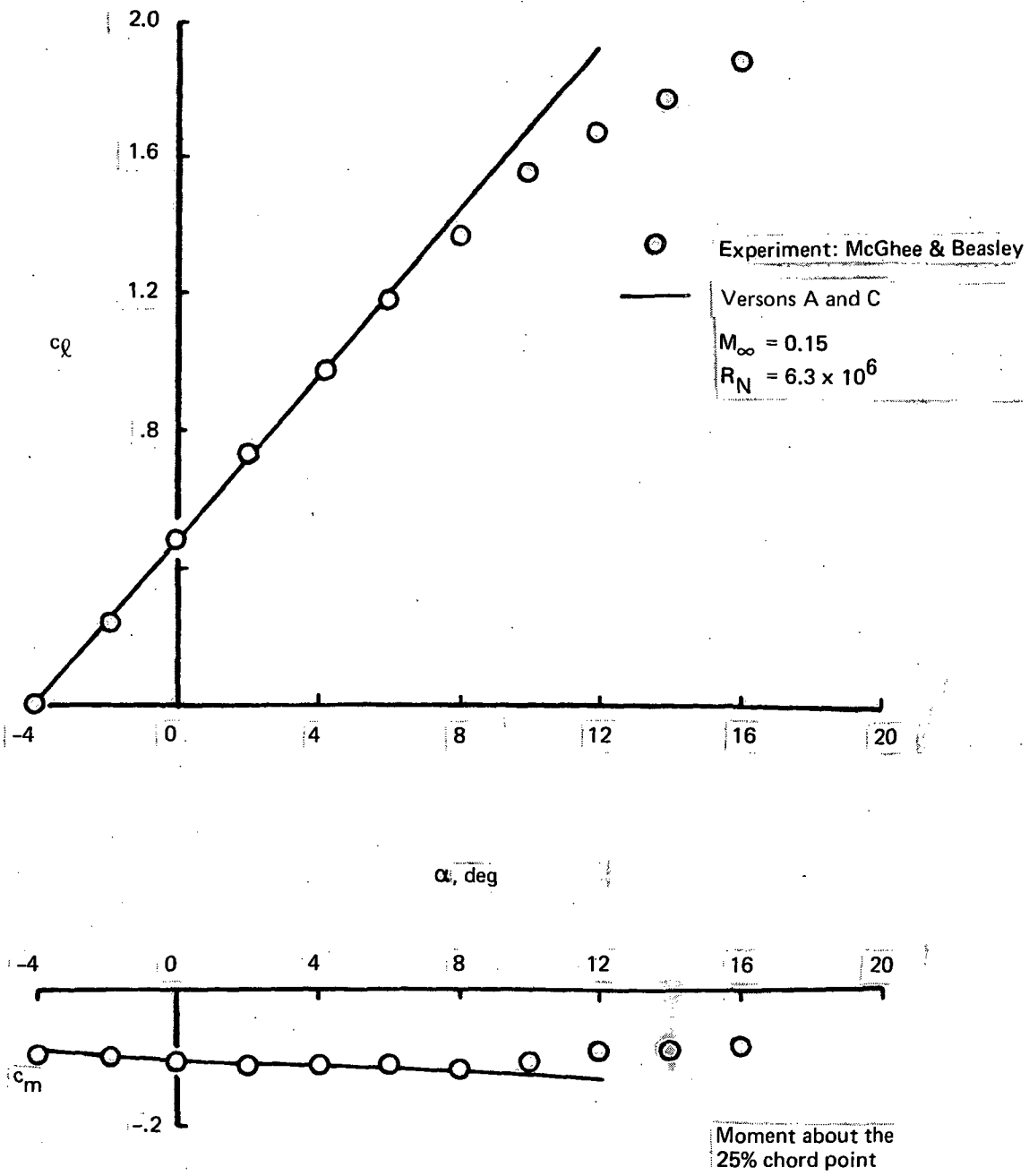


Figure 3. — Lift and Pitching Moment of GA(W)-1 Single Airfoil

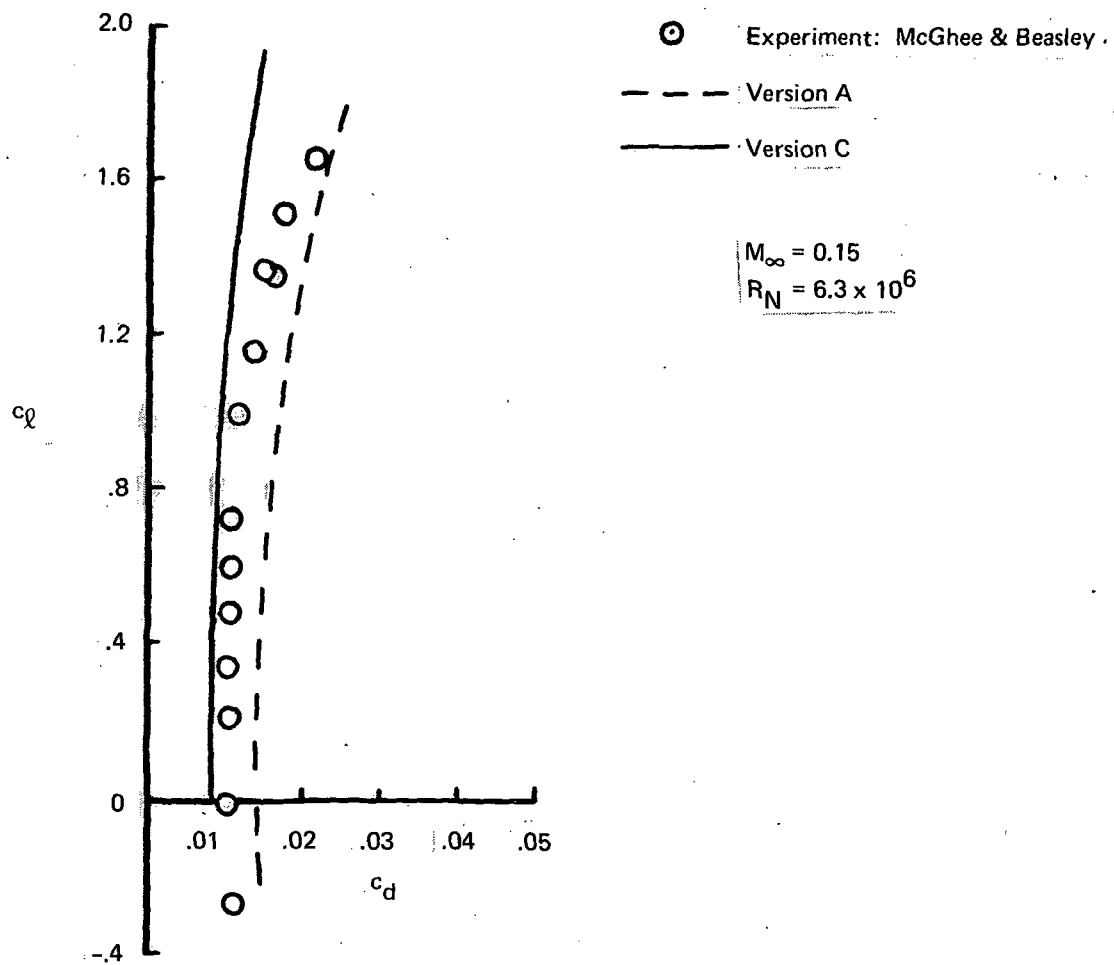


Figure 4. — Drag Polar of GA(W)-1 Single Airfoil

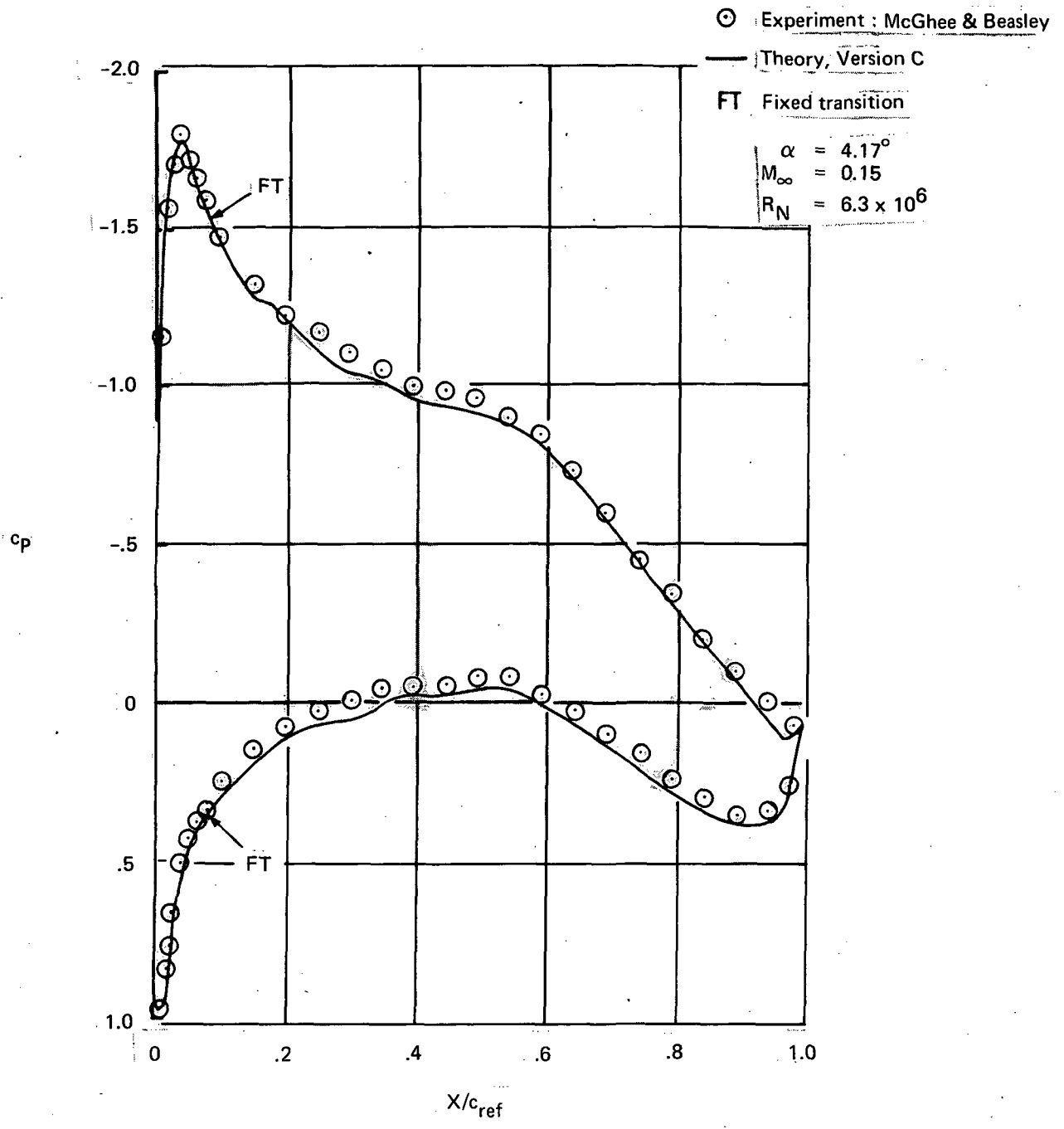
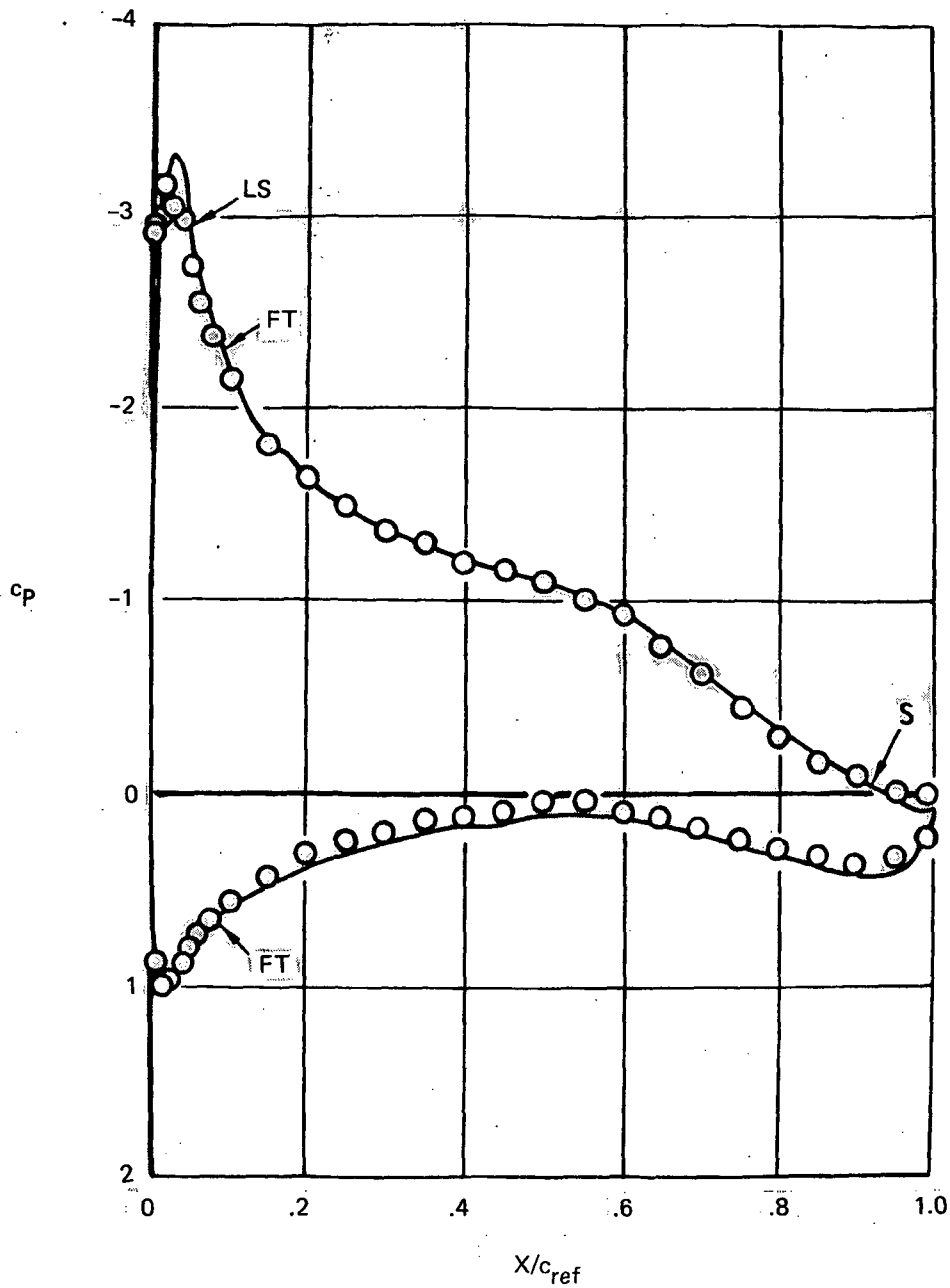


Figure 5. — Surface Pressures of GA(W)-1 Single Airfoil



- Experiment: McGhee & Beasley
  - Version C
  - FT Fixed transition
  - S Separation
  - LS Laminar short bubble
- $\alpha = 8.02^\circ$   
 $M_\infty = 0.15$   
 $R_N = 6.3 \times 10^6$

Figure 5. — (Concluded)

Note:  $\delta^*$ ,  $\theta$ ,  $\delta$ , are parameters of one side of the symmetric wake.

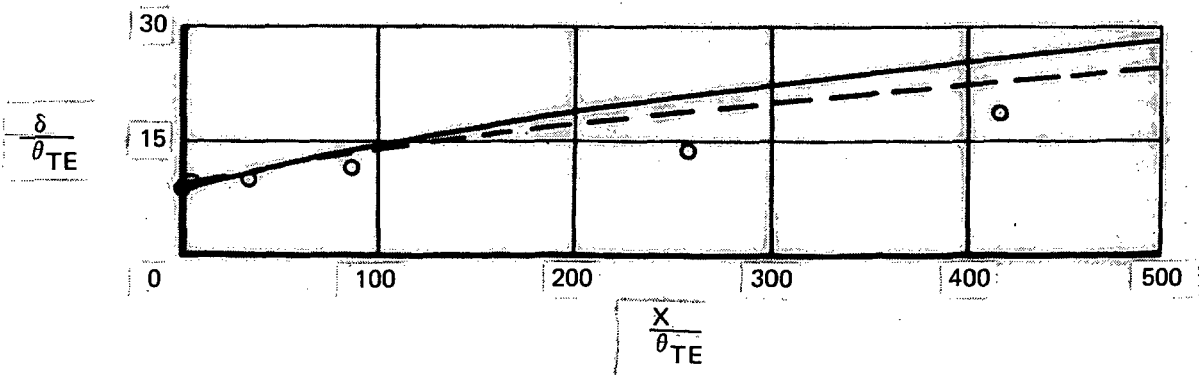
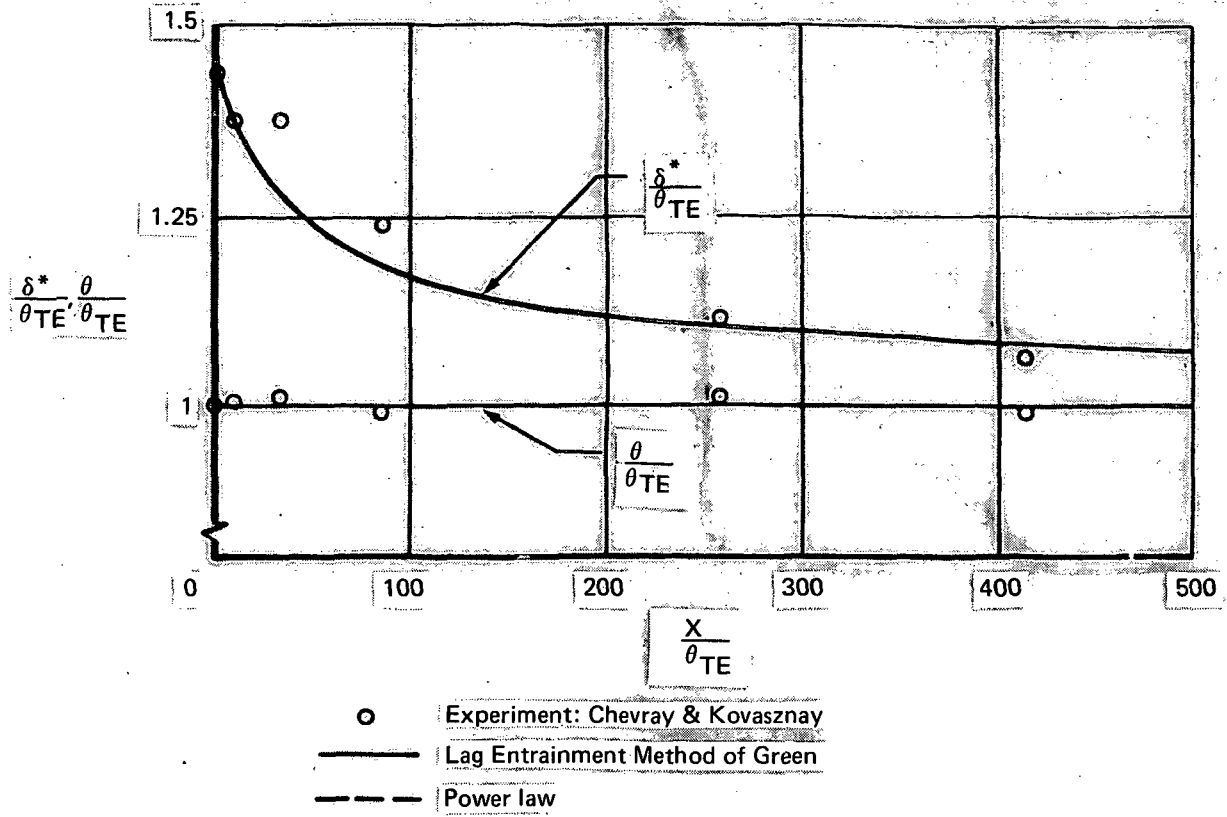


Figure 6. — Flat Plate Wake Characteristics

10 and 11); and appear to be the only available test results of two-dimensional wake characteristics at low-subsonic speeds. The agreement of theoretical and experimental wake parameters seems to be adequate for the present purpose, but better results for the wake displacement effect immediately downstream of the trailing edge might be desirable.

## TWO-ELEMENT AIRFOILS

### GA(W)-1 WITH 30% CHORD FLAP

The GA(W)-1 airfoil, with a single 30% chord trailing edge flap, served as the principal test case for this type of general aviation high lift airfoil. The experimental data were measured by Wentz, Seetharam, and Fisco (refs. 12, 13, and 14). The data include global airfoil parameters, detailed surface pressures, and boundary layer characteristics.

Figure 7 shows the lift and pitching moment characteristics of this airfoil with a flap deflection of  $10^\circ$ . The computed data of Version C agree very well with the experimental results in the prestall angle of attack range; Version B slightly mispredicts lift and moment curves. Figure 8 presents the lift curves at three different flap settings up to  $\delta_F = 30^\circ$  flap angle.

Figure 9 shows the corresponding pitching moment characteristics. The agreement of the theoretical data with the experiment is only satisfactory at lower angles of attack and lower flap angles. The differences at higher angles of attack are due to trailing edge stall, a phenomenon that is not modeled by the computer program.

The discrepancy between theoretical and experimental lift coefficients at the  $30^\circ$  flap angle and small angles of attack is unexpected in view of the good agreement between the theoretical and experimental pressure distributions (fig. 10). Furthermore, the experimental pressures do not indicate separation on the upper surface of the flap at small angles of attack. Hence, trailing edge stall can not be responsible for the observed disagreement.

Figure 11 shows a large discrepancy between theoretical and experimental drag polars. Presently, one can only speculate about the cause of the observed differences. None of the drag polars shown in the figure is believed to be correct for the following reasons: the theoretical values of lift and drag were computed on the basis of a model with many simplifying assumptions; the validity of some of these assumptions is questionable. A case in point is the computation of profile drag applying the Squire and Young formula, which is a crude approximation for high lift airfoils and, therefore, is not expected to produce very accurate results.

On the other side, the accuracy of the experimental drag polars of figure 11 must also be questioned. The data were obtained from a two-dimensional insert in a larger wind tunnel with no blowing or suction of the wall boundary layer applied. Boundary layer separation in the corners formed by the flap and the insert walls most likely took place at higher flap deflections and higher angles of attack, thereby causing a deviation from the desired two-dimensional flow pattern. Many of the flow visualizations published in reference 12 support this observation.

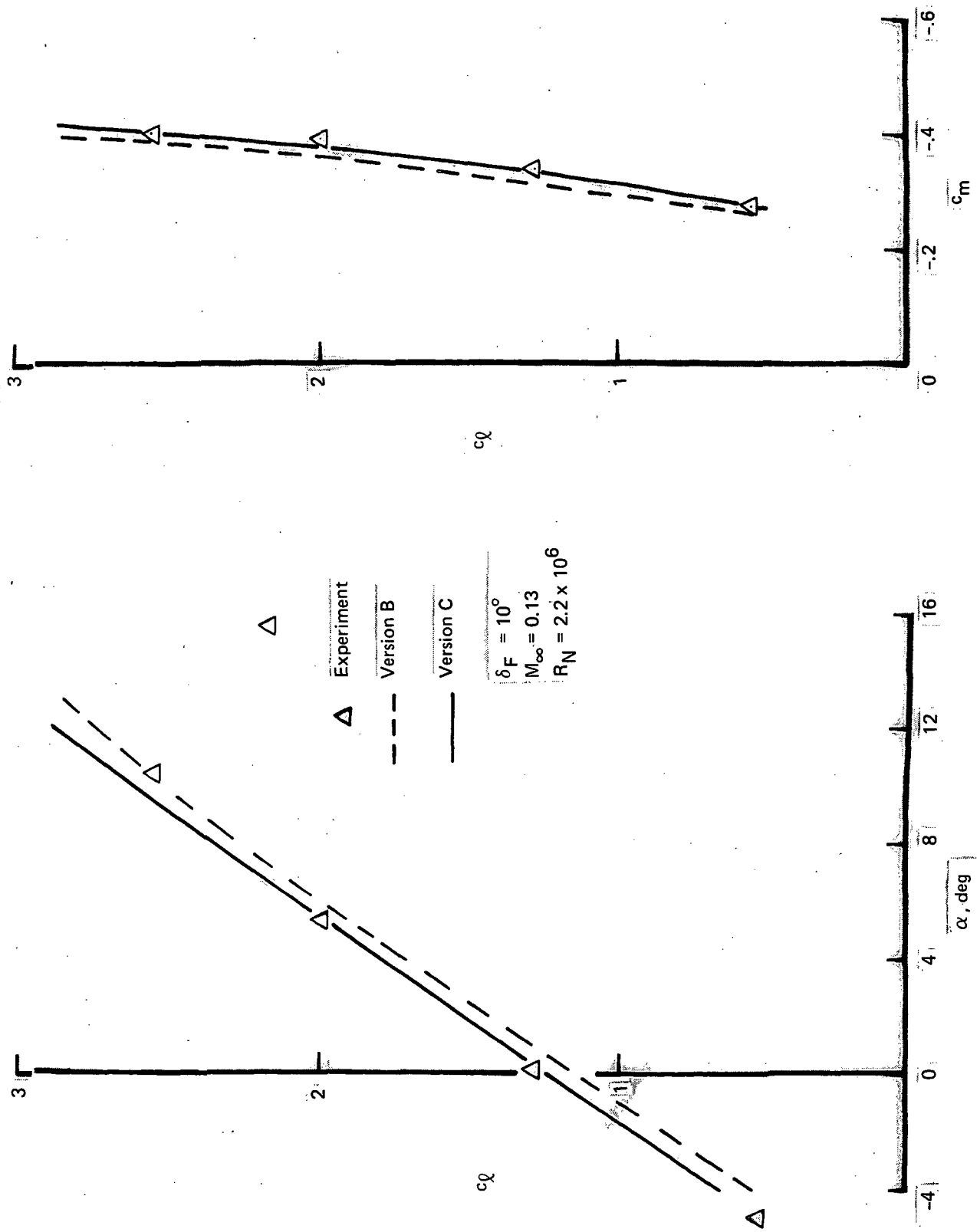


Figure 7. — Lift and Pitching Moment Characteristics of GA(W)-1 With 30% Chord Flap

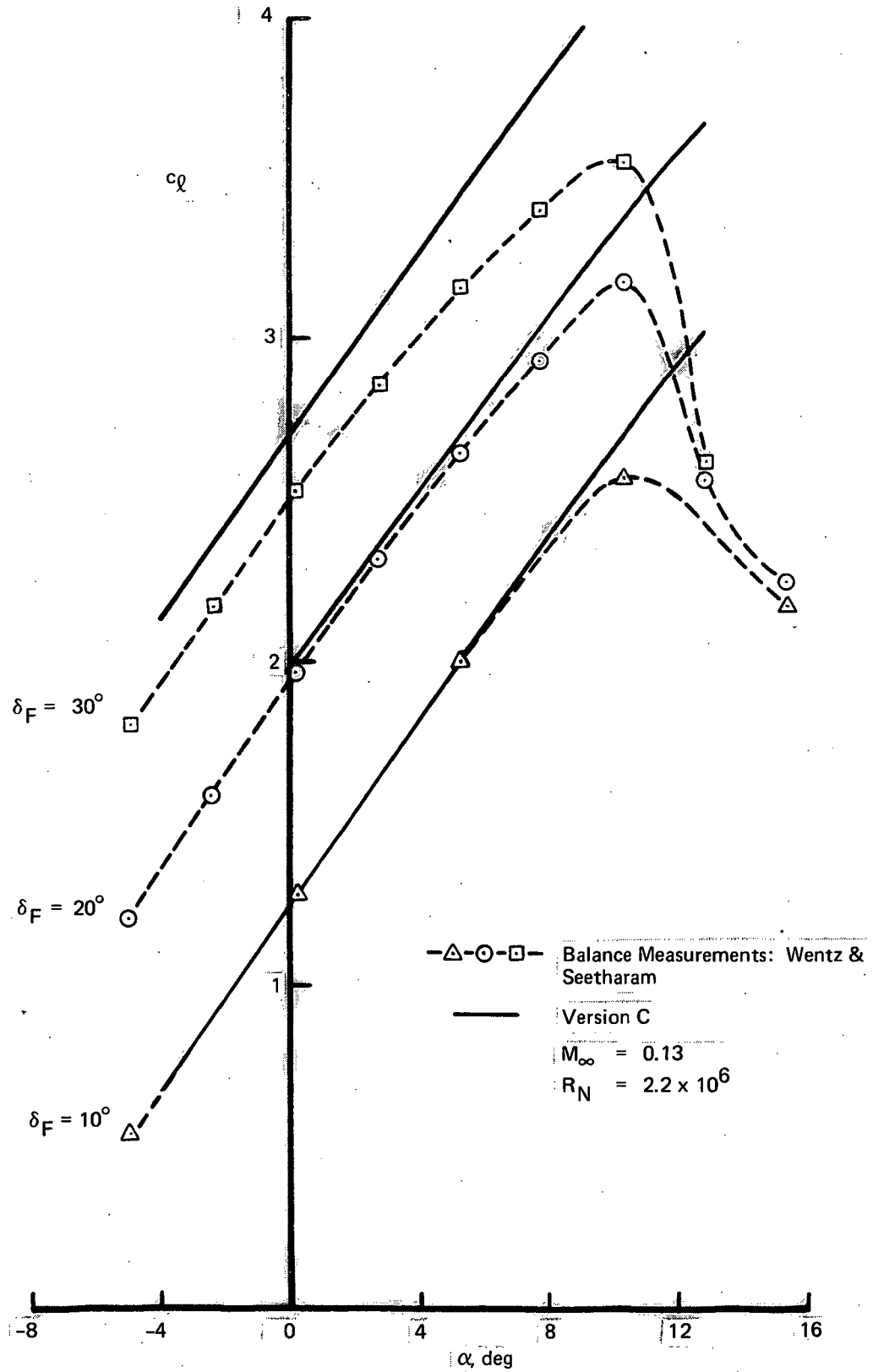


Figure 8. — Lift Curves of GA(W)-1 With 30% Chord Flap

△ ○ □ Experiment: Wentz & Seetharam

— Version C

$M_\infty = 0.13$

$R_N = 2.2 \times 10^6$

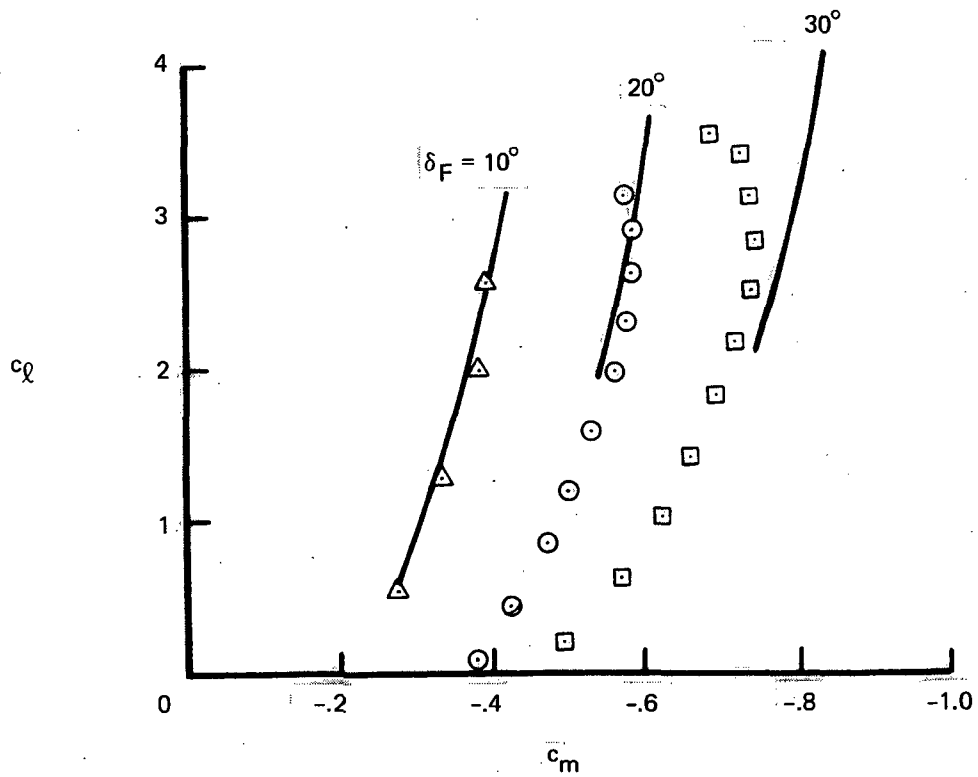


Figure 9. — Pitching Moment Characteristics of GA(W)-1 With 30% Chord Flap

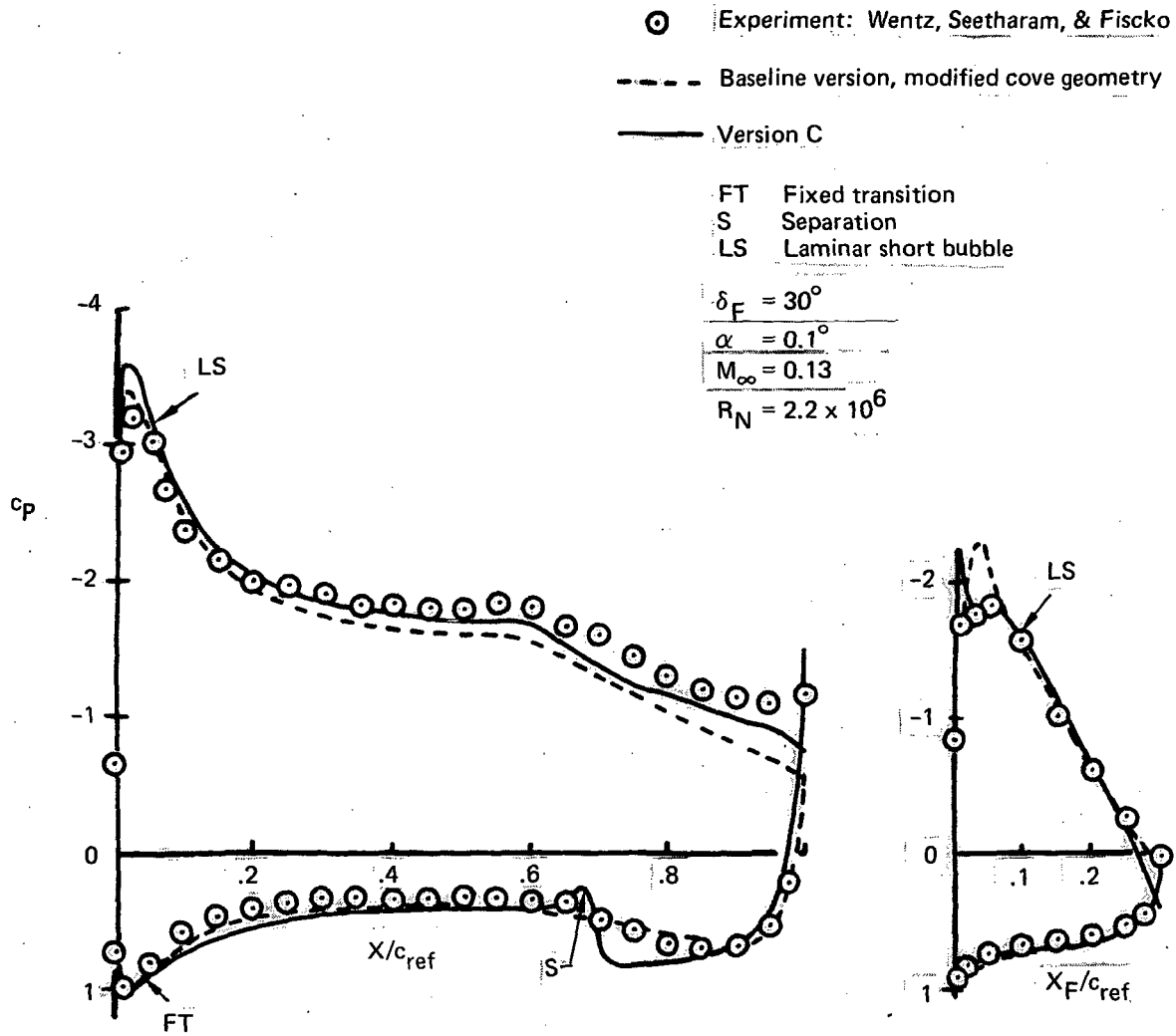


Figure 10. — Surface Pressure of GA(W)-1 With 30% Chord Flap

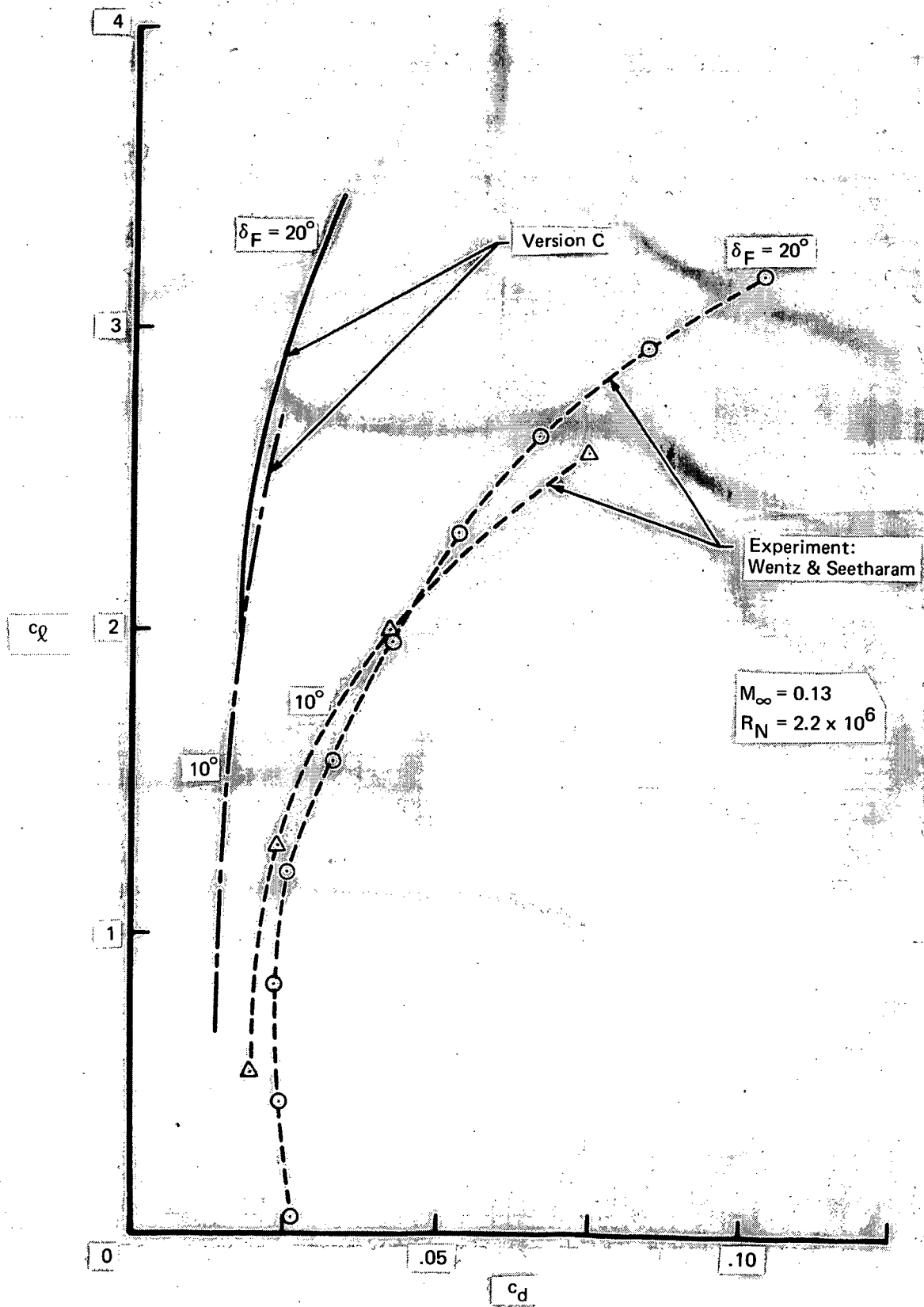


Figure 11. — Drag Polar of GA(W)-1 With 30% Chord Flap

Pressure distributions are compared in figure 12 for the 20° flap angle and in figure 10 for the 30° case. The solid lines represent the theoretical predictions of Version C which reasonably well approximate the experimental surface pressures in all cases. Differences are observed in the cove region and near the upper surface trailing edge. Mispredictions are expected from an aerodynamic theory that does not attempt to properly model the recirculating flow in this region. No explanation is offered for the discrepancy between theoretical and experimental pressure distributions near the upper surface trailing edge. Figure 12 further shows theoretical results of the baseline version of the code obtained by Wentz, Seetharam, and Fisco (ref. 13). The cove geometry of the GA(W)-1 had been modified by these authors to produce a better match of theory and experiment in the cove region. At this point it should be emphasized that all other comparisons shown in this document are based on the true airfoil geometries without modifications.

The computed boundary layer thickness (Version C) on both surfaces of the main component of the GA(W)-1 high lift airfoil is shown in figure 13. The boundary layer thickness  $\delta_u$  on the upper surface grows continuously, whereas,  $\delta_l$  on the lower surface suddenly increases at the entrance to the cove and later nearly vanishes at the lower surface trailing edge. This thickening of the boundary layer has been noticed in all theoretical results and seems, at least qualitatively, to be a realistic description of the flow pattern in the cove region. The boundary layer at the lower surface trailing edge is too thin which results in erroneous initial values for the subsequent calculation in the core region. The potential core size is overestimated at the slot exit which in turn shifts the end of the core region too far downstream.

Figure 14 through 19 contain data of the GA(W)-1 with a 30% chord trailing edge flap at 40° flap angle. Experimental data (ref. 14) clearly shows separation on the flap upper surface for this configuration. Presumably this is the reason theoretical and experimental lift coefficients disagree (fig. 14). The pressure distributions of figure 15 verify the separated flow condition on the upper surface of the flap. In this area, the theoretical pressure data do not agree well with measured pressures as large scale flow separation is not modeled by the program. The agreement is better along the surface of the main airfoil component, but substantial differences are noted near the upper surface leading edge and, as already observed at lower flap settings, in the cove region. The reader should note that program Version C produces more accurate pressures on the second half of the upper surface, due to better representation of boundary layer displacement effects in the potential flow part. Program Version A accounted for displacement effects by modifying the camberline of the airfoil. This resulted in an unrealistic coupling of upper and lower surface pressure distributions that can clearly be seen in figure 15.

Figure 16 presents a comparison of skin friction coefficients on the upper surface of the GA(W)-1. The corresponding predictions of the point of separation on the flap upper surface are shown in figure 17. Theoretically, separation is not well predicted, which is probably due to the misprediction of the pressures on the flap upper surface. Improvements will have to be made by properly modeling large scale separation.

⊙ Experiment: Wentz, Seetharam, & Fisco

--- Baseline version, modified cove geometry

— Version C

FT Fixed transition

S Separation

LS Laminar short bubble

$$\delta_F = 20^\circ$$

$$\alpha = 0.2^\circ$$

$$M_\infty = 0.13$$

$$R_N = 2.2 \times 10^6$$

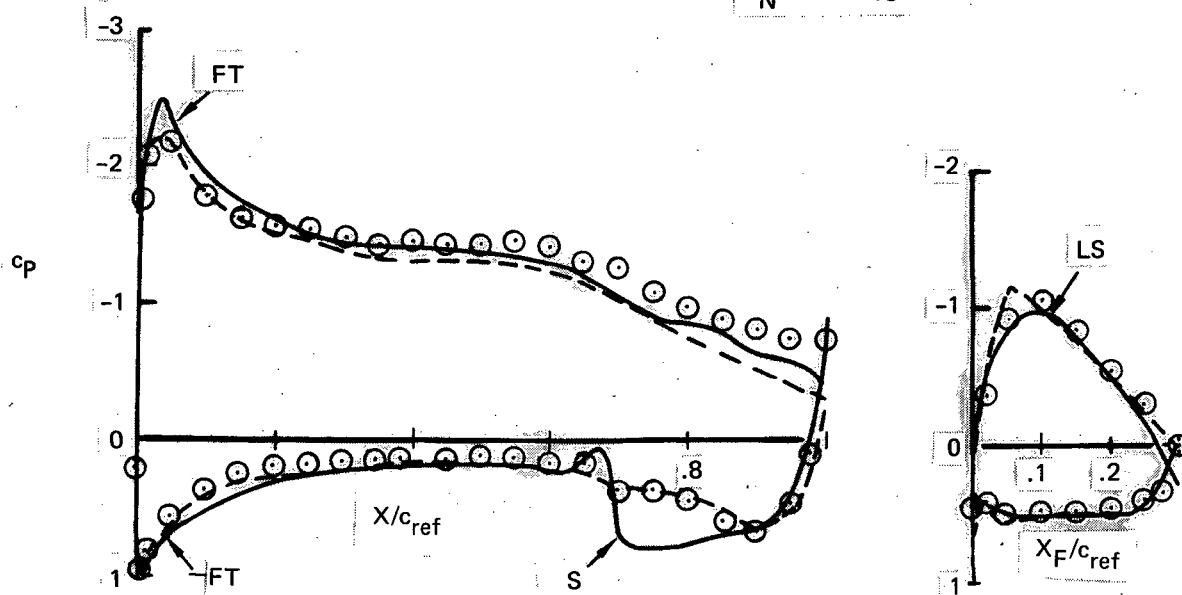


Figure 12. — Surface Pressure of GA(WO-1 With 30% Chord Flap

⊙ Experiment: Wentz, Seetharam, & Fisco

--- Baseline version, modified cove geometry

— Version C

FT Fixed transition

S Separation

LS Laminar short bubble

$$\delta_F = 20^\circ$$

$$\alpha = 5.2^\circ$$

$$M_\infty = 0.13$$

$$R_N = 2.2 \times 10^6$$

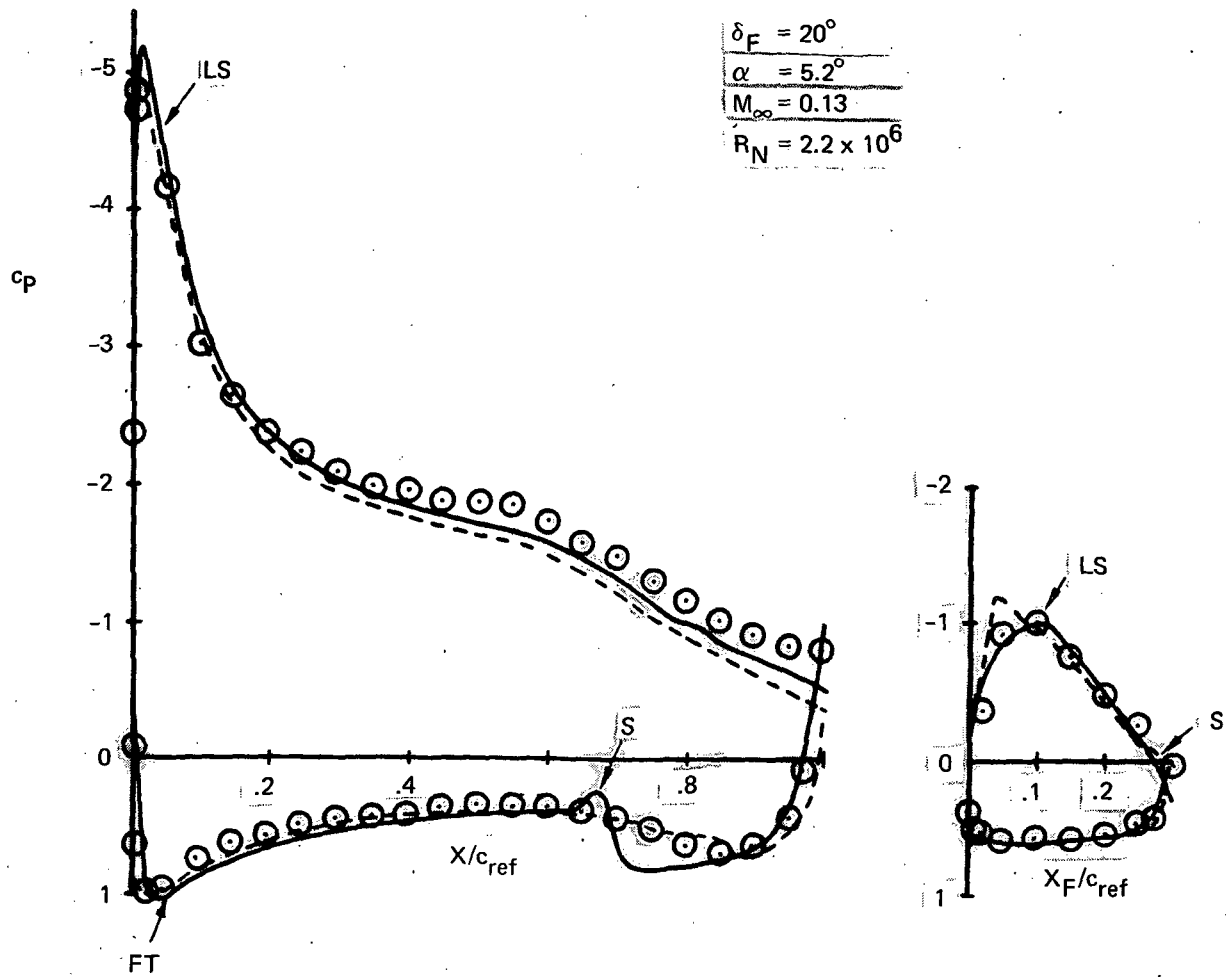


Figure 12. - (Continued)

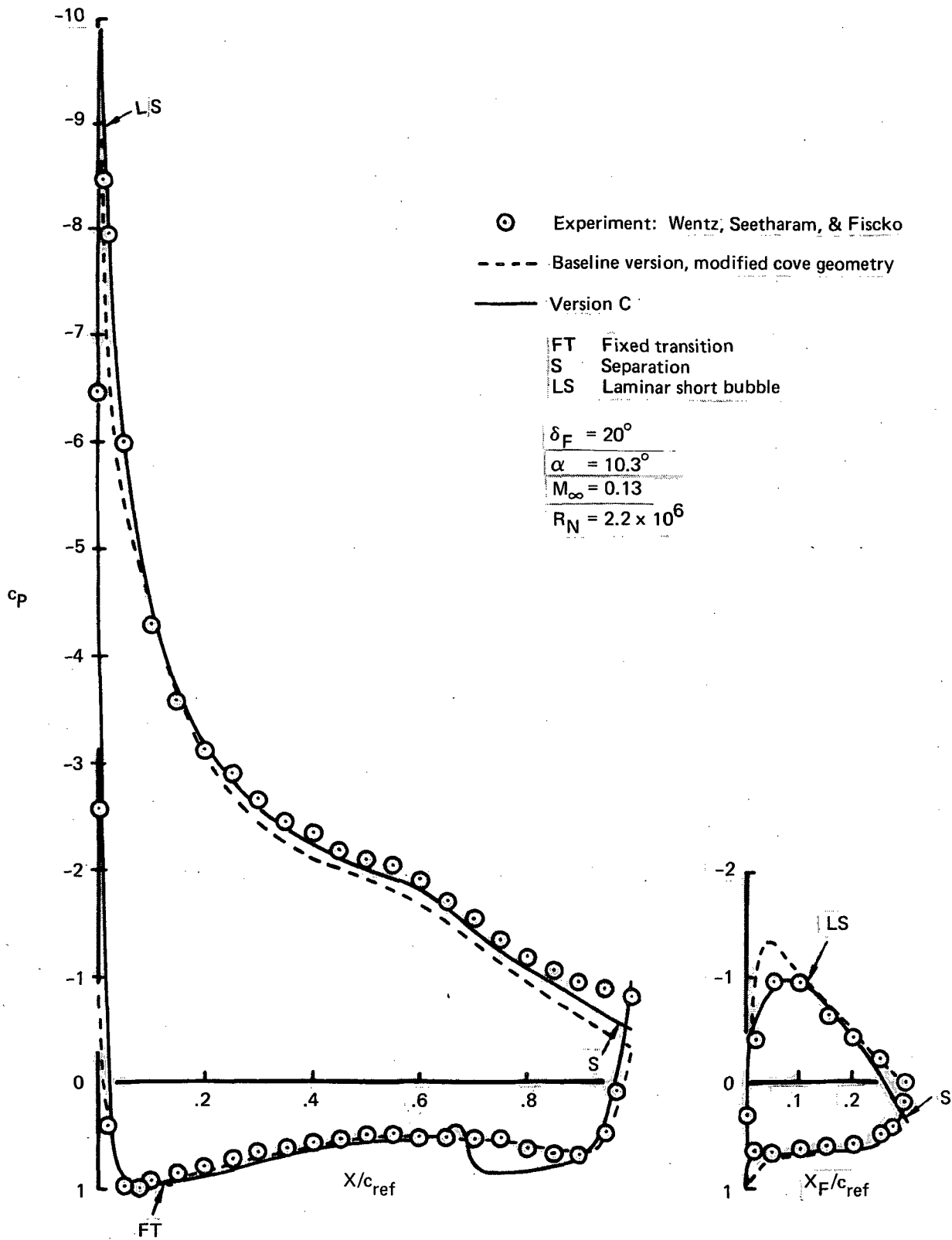


Figure 12. - (Concluded)

$\alpha = 5.2^\circ$   
 $M_\infty = 0.13$   
 $R_N = 2.2 \times 10^6$   
 $\delta_F = 20.0^\circ$

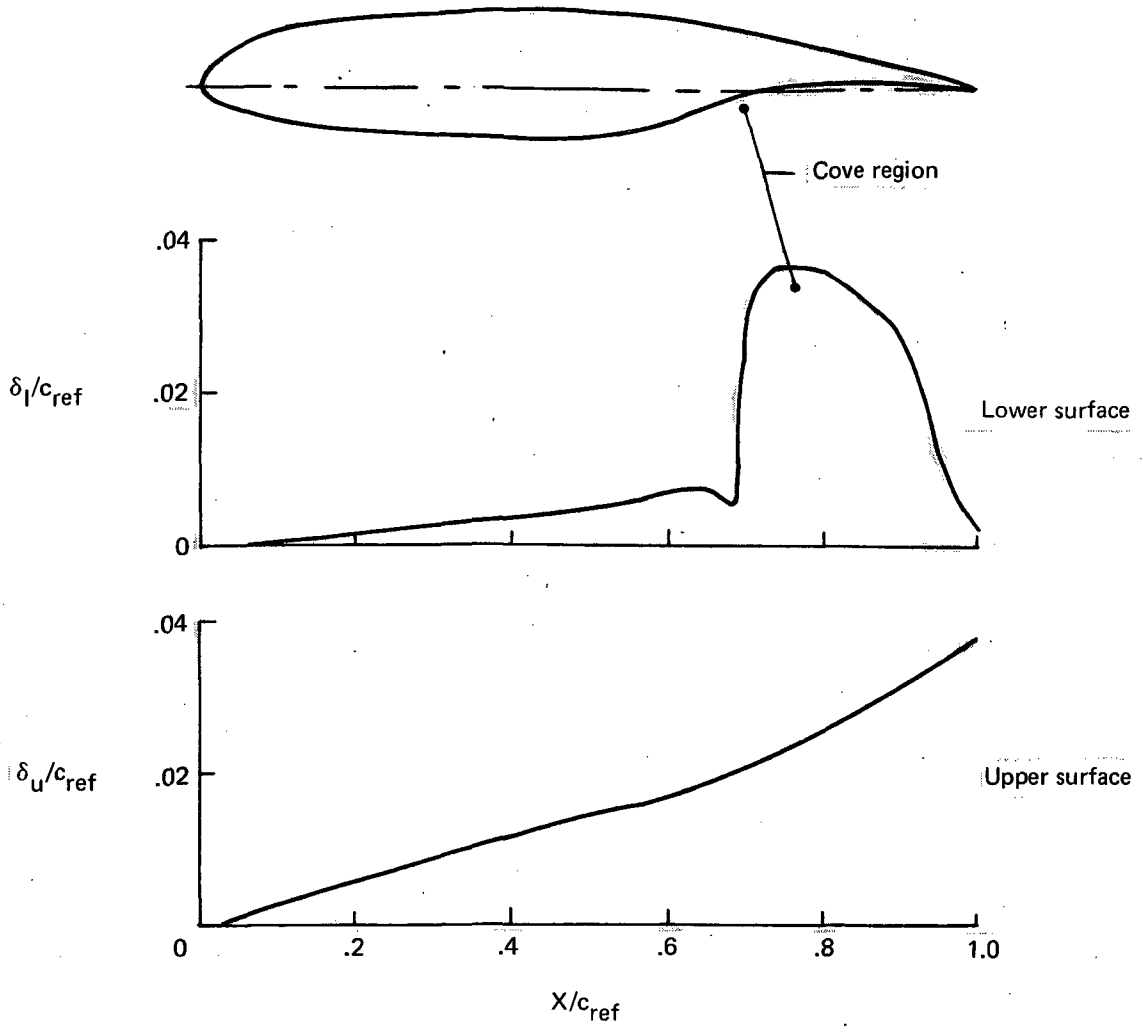


Figure 13. — Boundary Layer Thickness on Main Component of GA(W)-1 With 30% Chord Flap

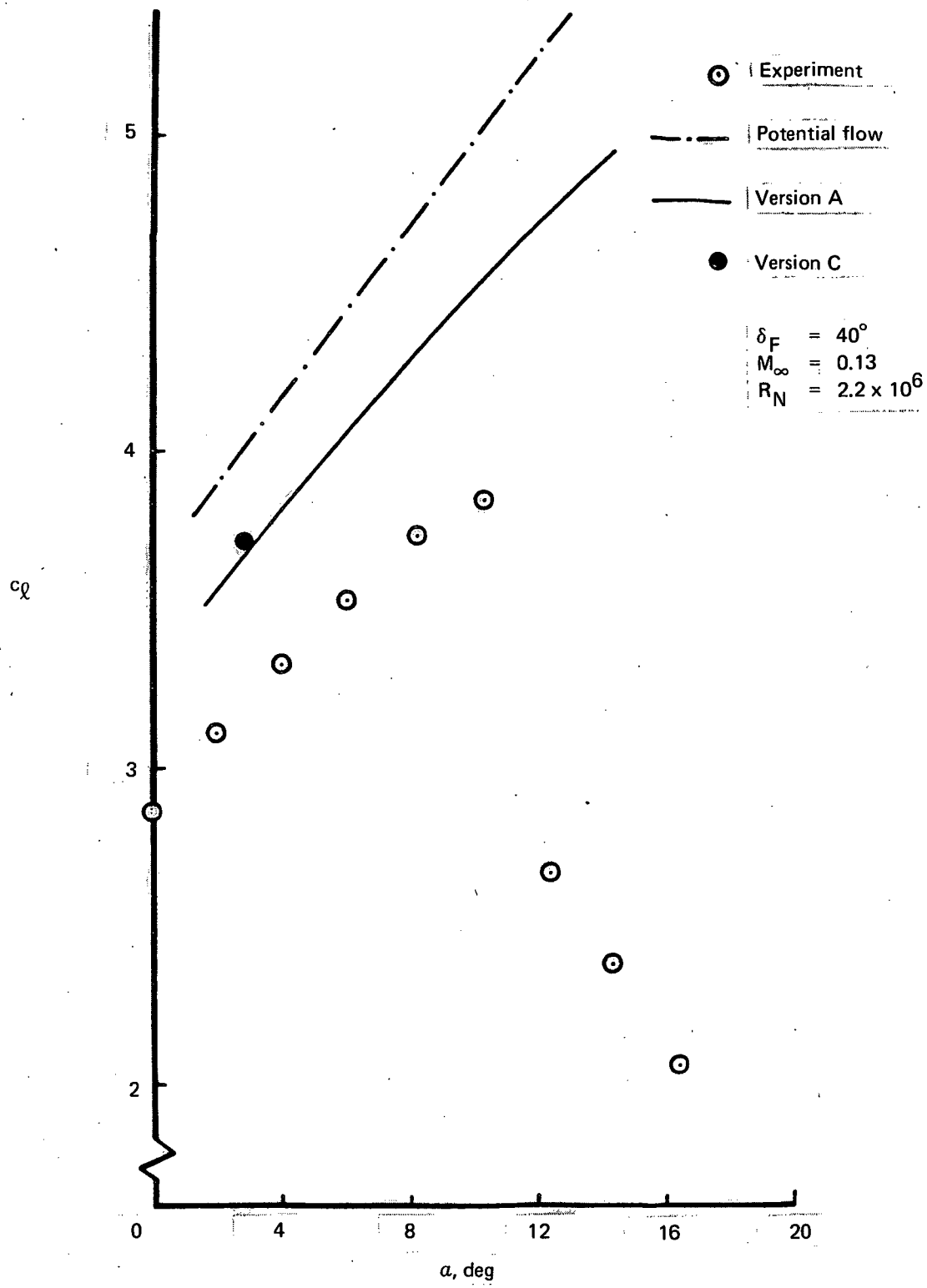


Figure 14. — Lift Curve of GA(W)-1 With 30% Chord Flap

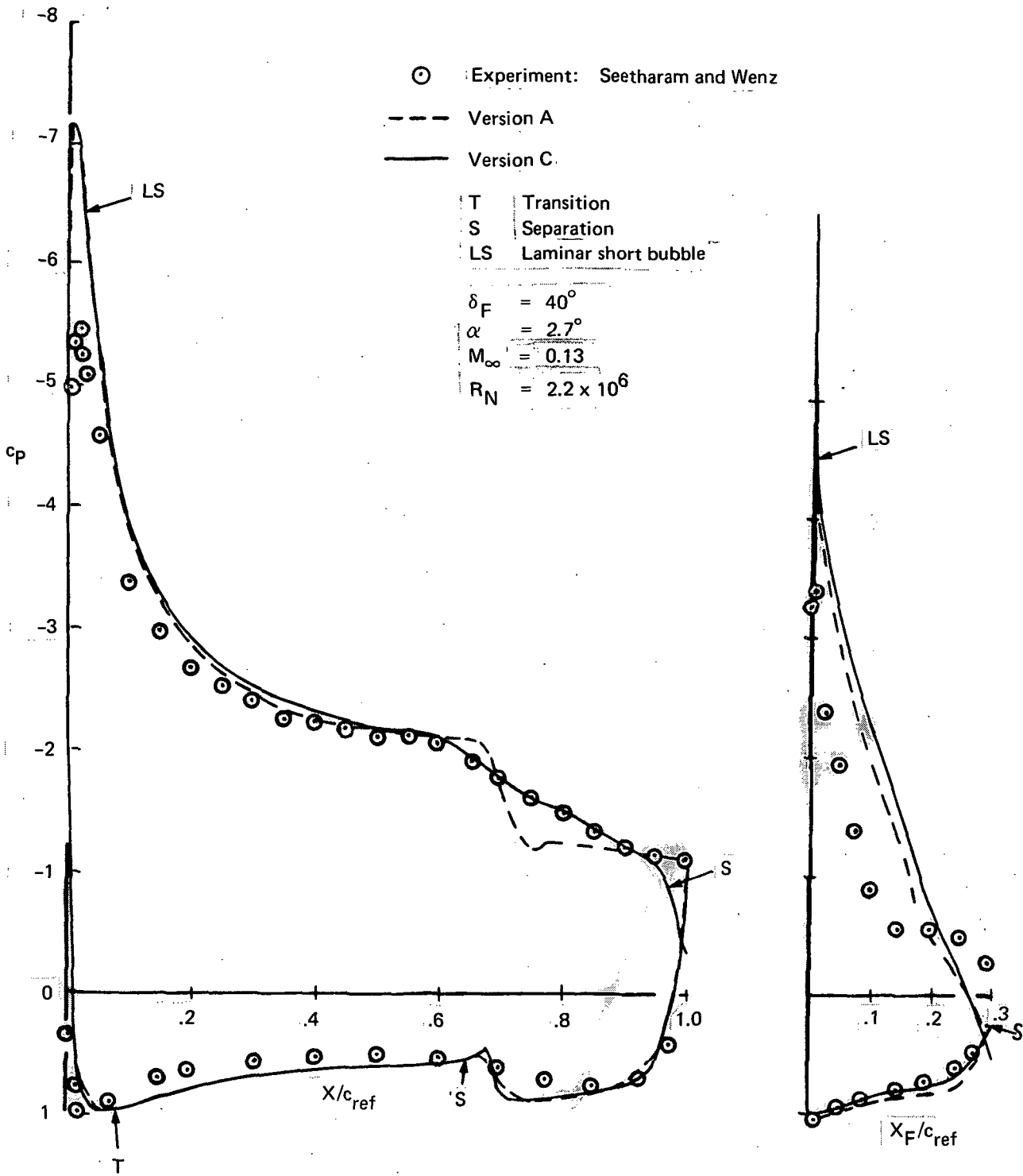


Figure 15. — Surface Pressure of GA(W)-1 With 30% Chord Flap

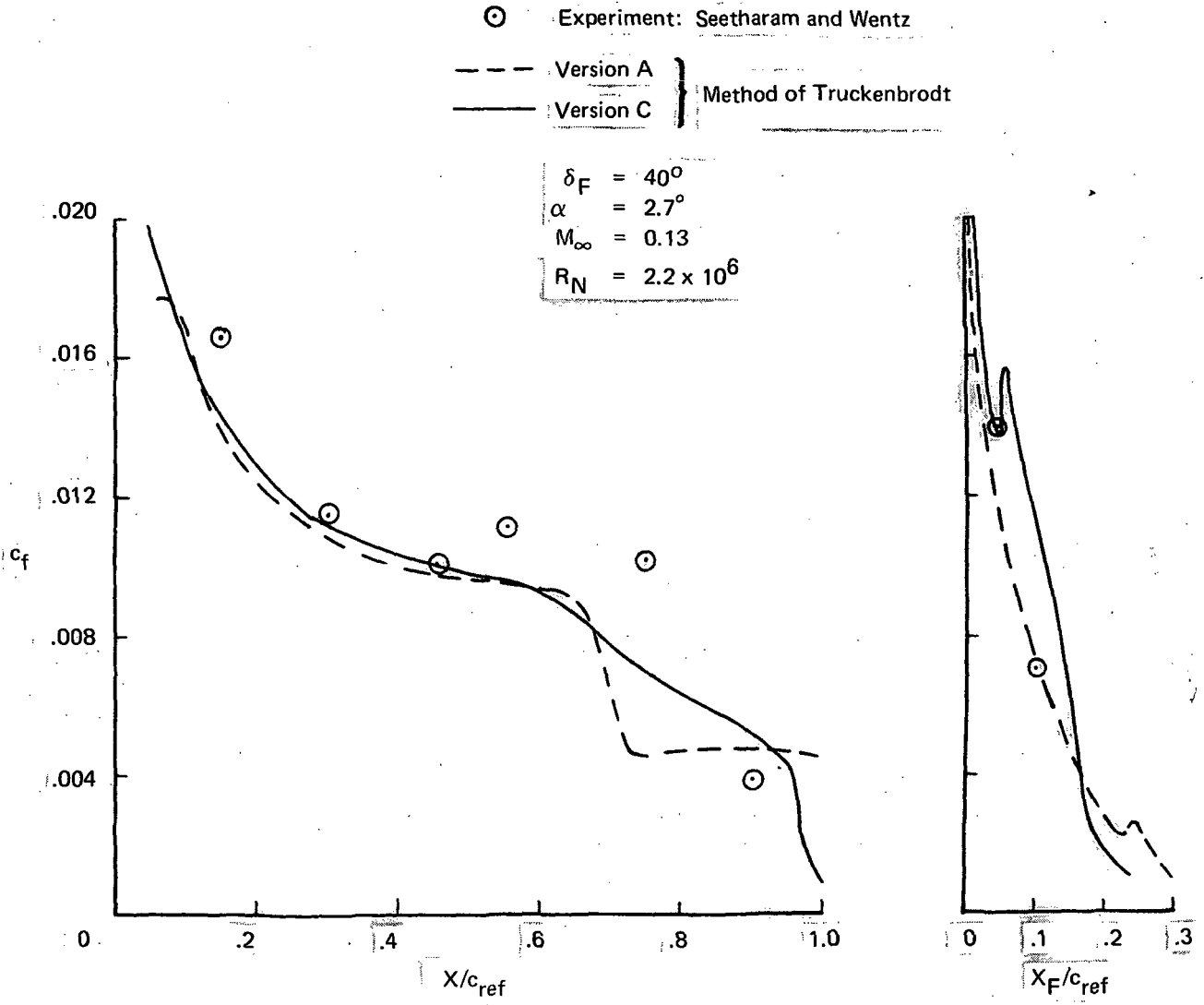


Figure 16. — Skin Friction on Upper Surface of GA(W)-1 With 30% Chord Flap

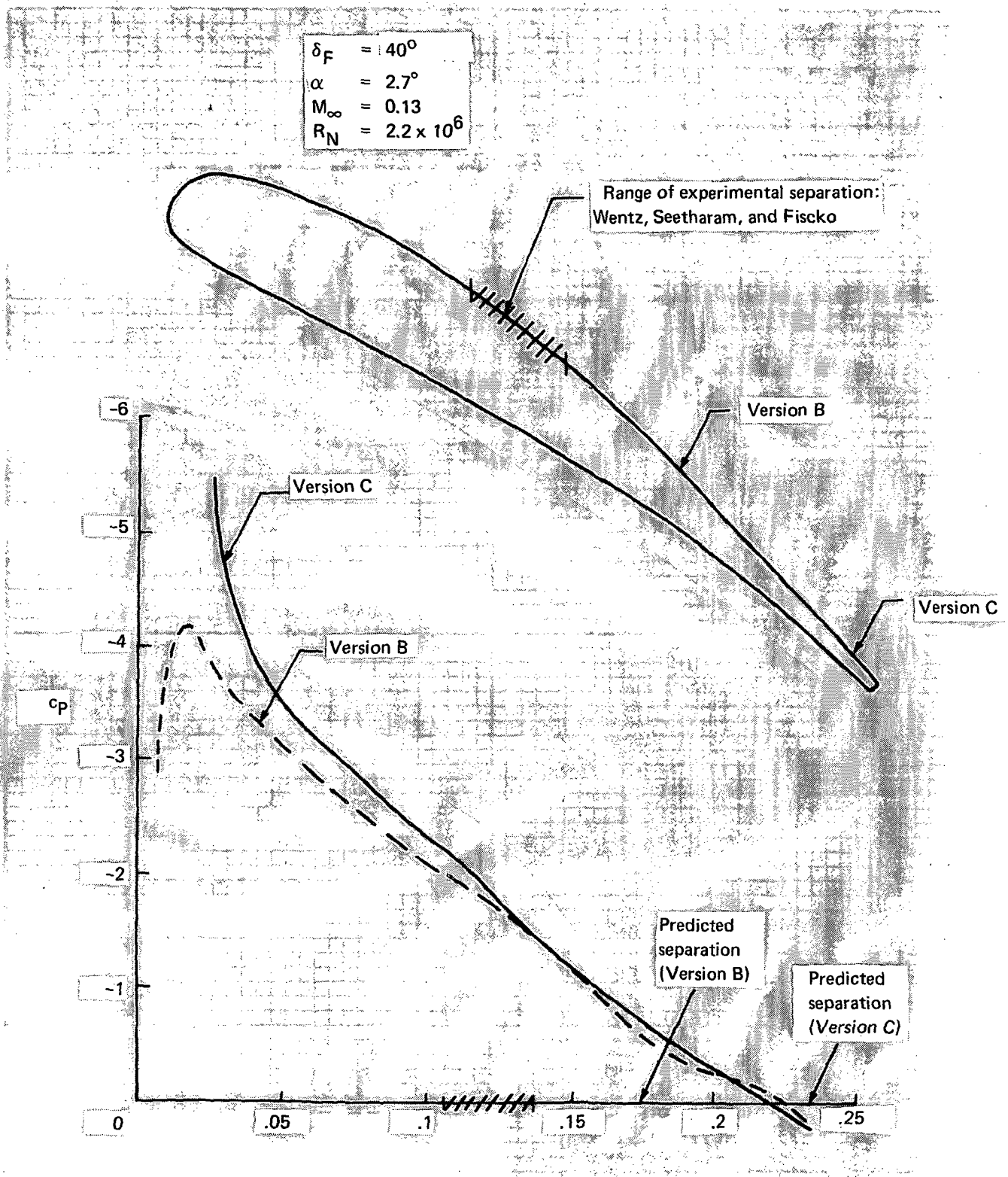


Figure 17. - Separation on Flap Upper Surface of the GA(W)-1 With 30% Chord Flap

Figure 18 again emphasizes the coupling of upper and lower surface data in the computations of program Version A. As shown earlier in figures 13 and 15, such a coupling of upper and lower surface data is not present in the theoretical prediction of Version C.

Figure 19 demonstrates the inability of the NASA-Lockheed program to simulate correctly separated flow. Even though theoretical results of Version A are only shown, this statement applies to all program versions.

#### **FOSTER'S AIRFOIL**

A few results for the two-element airfoil, Foster (ref. 15), are shown in figures 20 and 21. Theoretical and experimental pressure distributions are only in partial agreement and, also higher values of the boundary layer displacement thickness on the upper surface of the flap are estimated by Versions A and B of the program. Similar results were calculated by program Version C. The reasons for this discrepancy are not known. Most likely the correspondence between test data and airfoil configurations in Foster's publication (ref. 15) was misinterpreted since test results in the referenced document do not clearly define geometric parameters of the tested configurations (figs. 20 and 21). Furthermore, the Reynolds number and the Mach number are not stated and must be estimated on the basis of the given tunnel speed (table 2). For these reasons, Foster's high lift data are of limited value for an evaluation of the performance predictions of the computer program.

#### **LJUNGSTRÖM'S AIRFOIL**

Lift and drag coefficients of Ljungström's two-element airfoil (ref. 16) are shown in figure 22. Theoretical predictions of program Version B were only successful at a zero degree angle of attack, but did not converge to a solution at other angles. No attempt was made to use Version C for a performance analysis of Ljungström's airfoil.

### **FOUR-ELEMENT AIRFOILS**

#### **BOEING HIGH LIFT AIRFOIL**

The Boeing four-element high lift airfoil (fig. 1 and table 3) was used as the main test case for multiple airfoils. It consists of a wing section with a leading edge flap and a double slotted trailing edge flap. Global airfoil parameters and detailed distributions of surface pressures and boundary layer data are available for comparisons. The data were obtained in the Boeing research wind tunnel (BRWT) on a model with 2 feet unextended wing chord and 5 feet span. Careful blowing of the wall boundary layers was applied in order to achieve a two-dimensional flow pattern across the whole span of the airfoil.

The lift curve and the drag polar of this airfoil at a Reynolds number of two million, based on the wing reference chord, are given in figures 23 and 24. The experimental lift coefficients are balance data that are within 1.5% of the lift obtained by pressure integration. The profile drag of the airfoil is the result of wake rake measurements taken at a fixed spanwise position relatively free from interference effects of flap

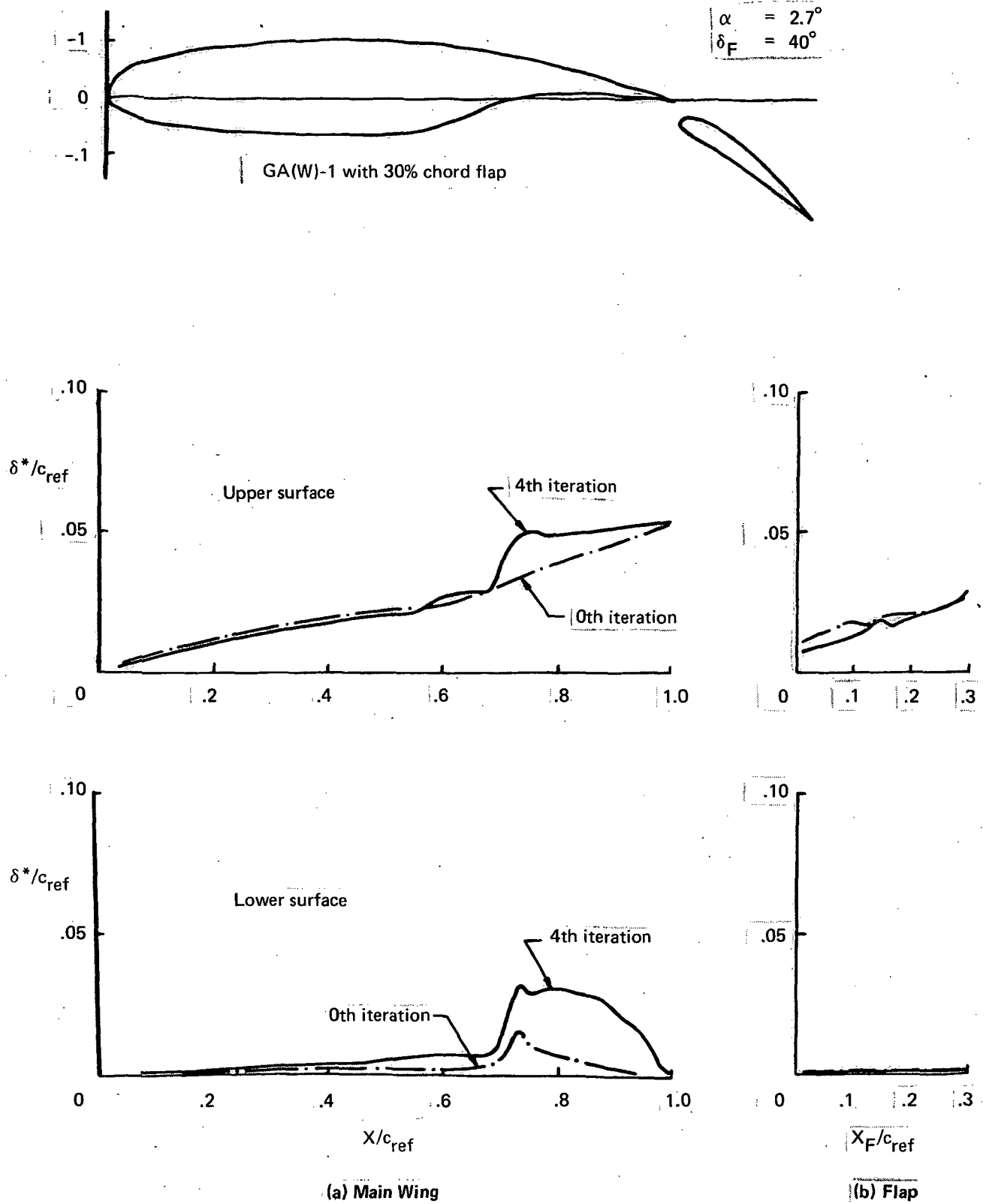


Figure 18. — Variation of Displacement Thickness During Iteration of Version A for GA(W)-1

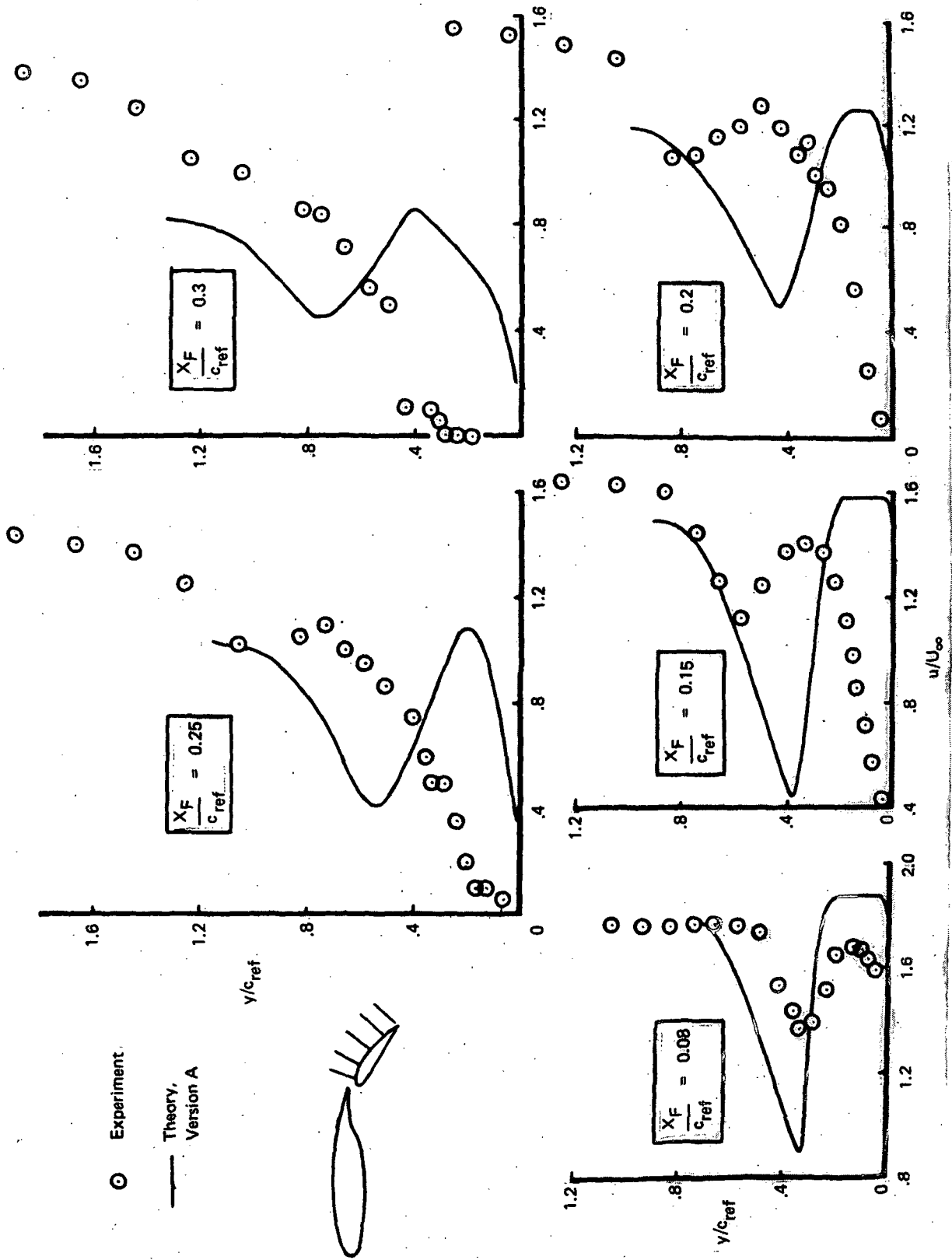


Figure 19. — Boundary Layer Profiles, Comparison of Theory and Experiment for GA(W)-1  
 With 30% Chord Flap,  $\alpha = 2.7^\circ$ ,  $\delta_F = 40^\circ$

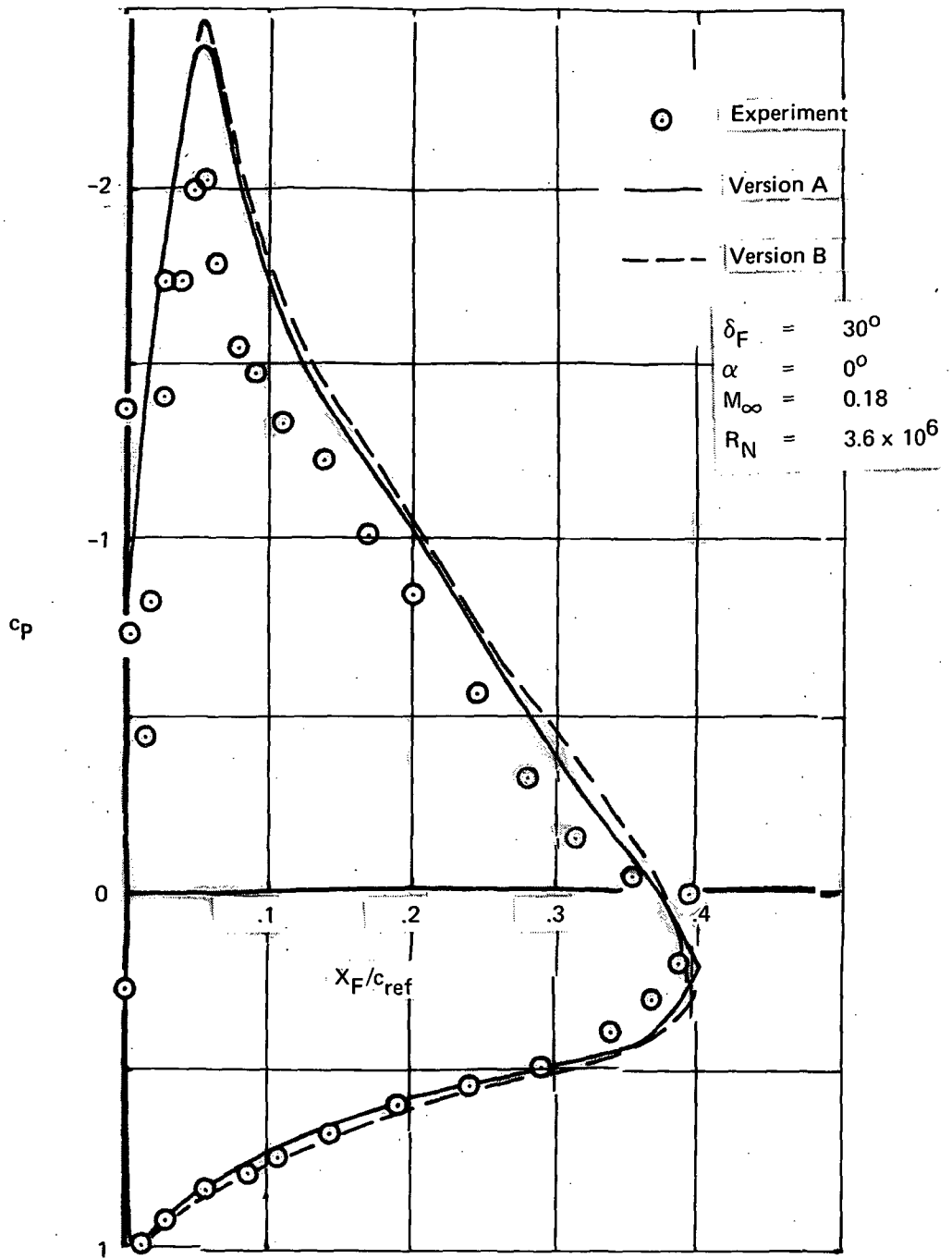


Figure 20. — Pressure Distribution on Flap for Foster Two-Element Airfoil

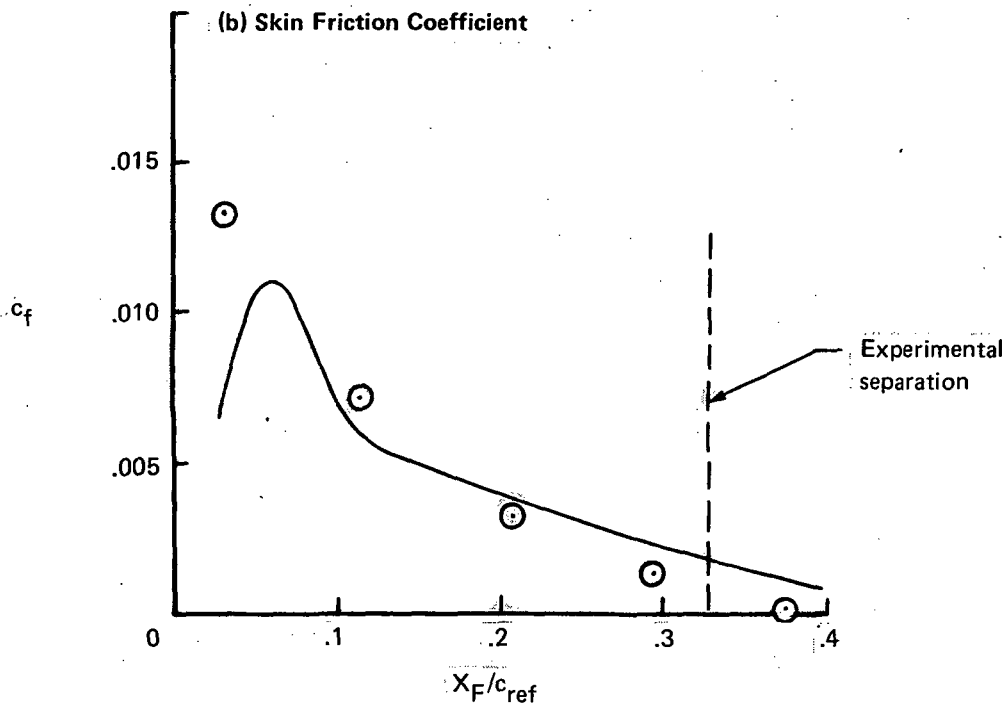
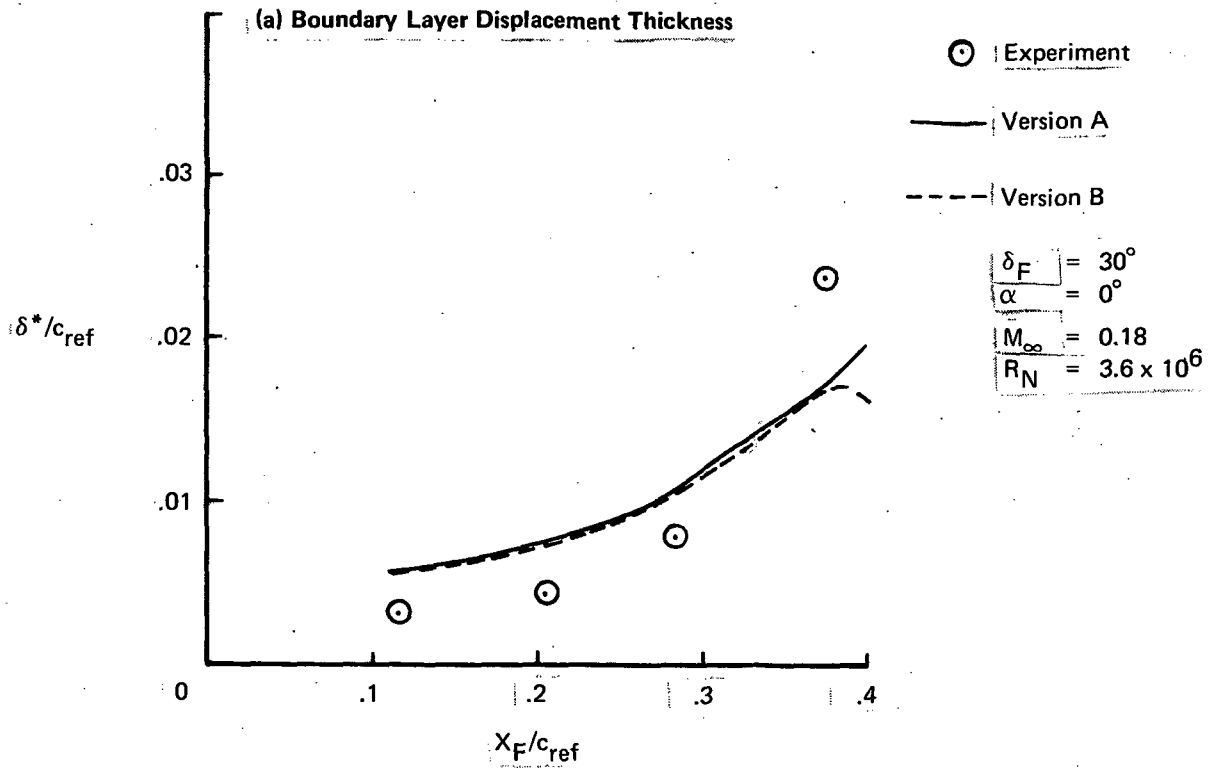


Figure 21. — Boundary Layer Parameters on Flap Upper Surface of Foster Two-Element Airfoil

Configuration 1

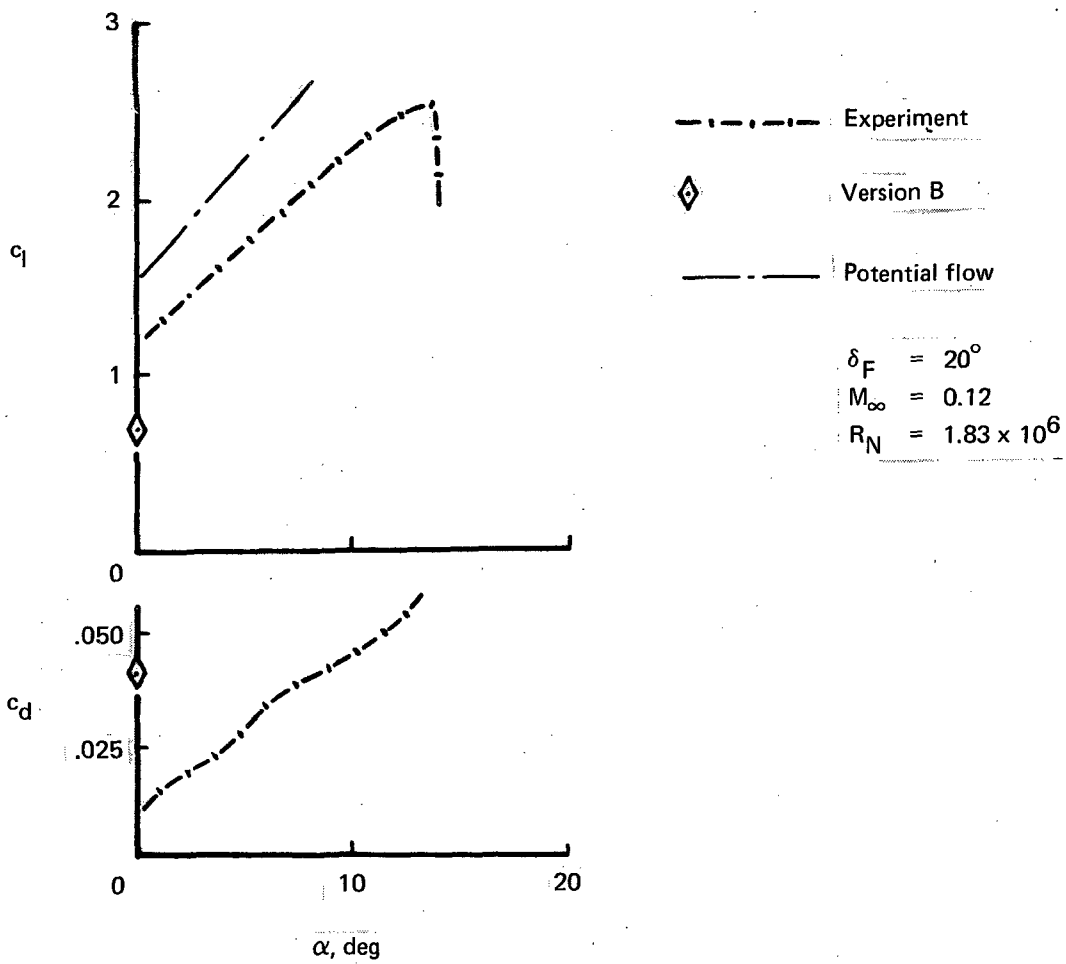


Figure 22. — Lift and Drag Comparison for Ljungström Two-Element Airfoil

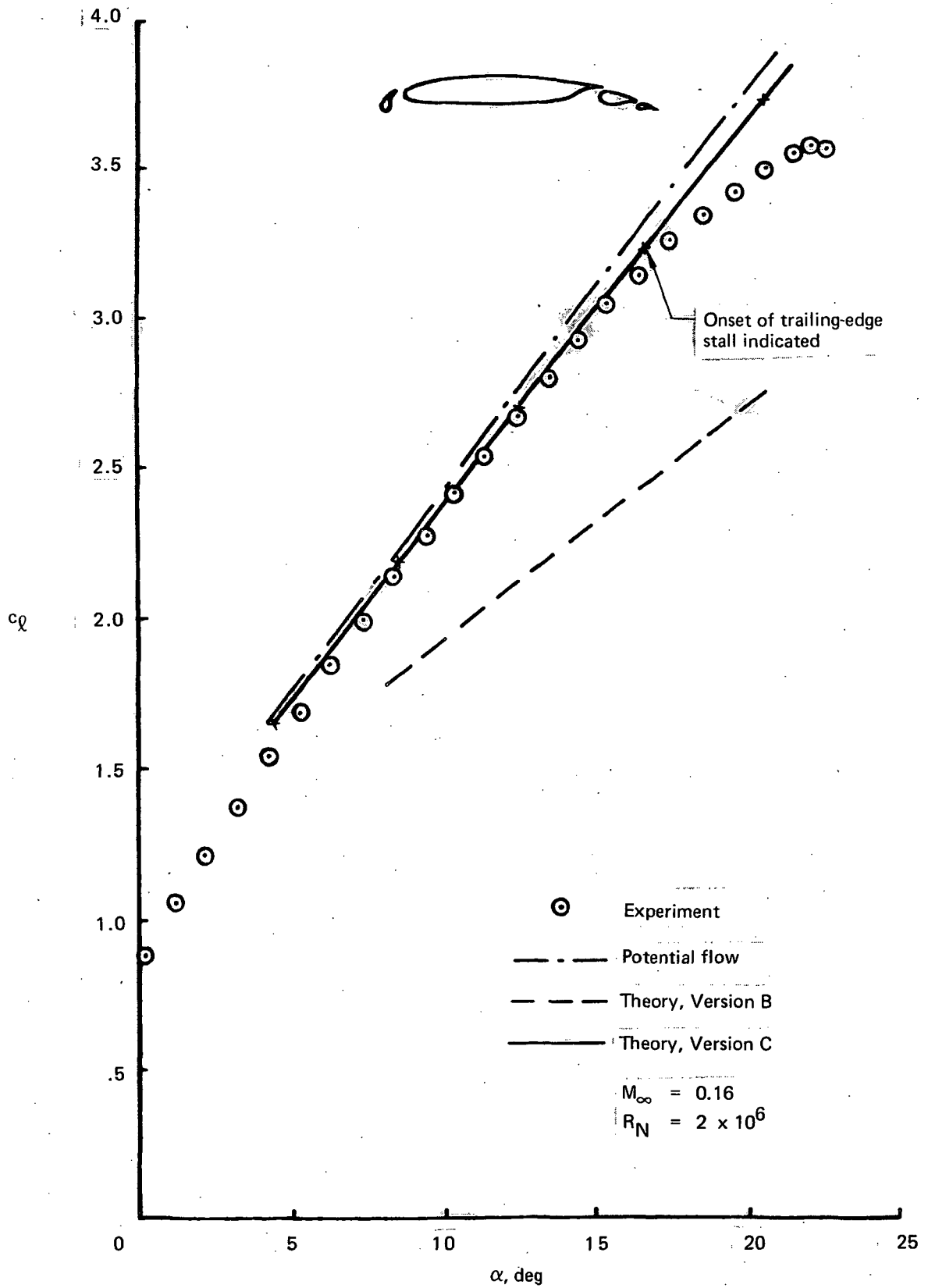


Figure 23. — Lift Curve of Boeing Four-Element Airfoil

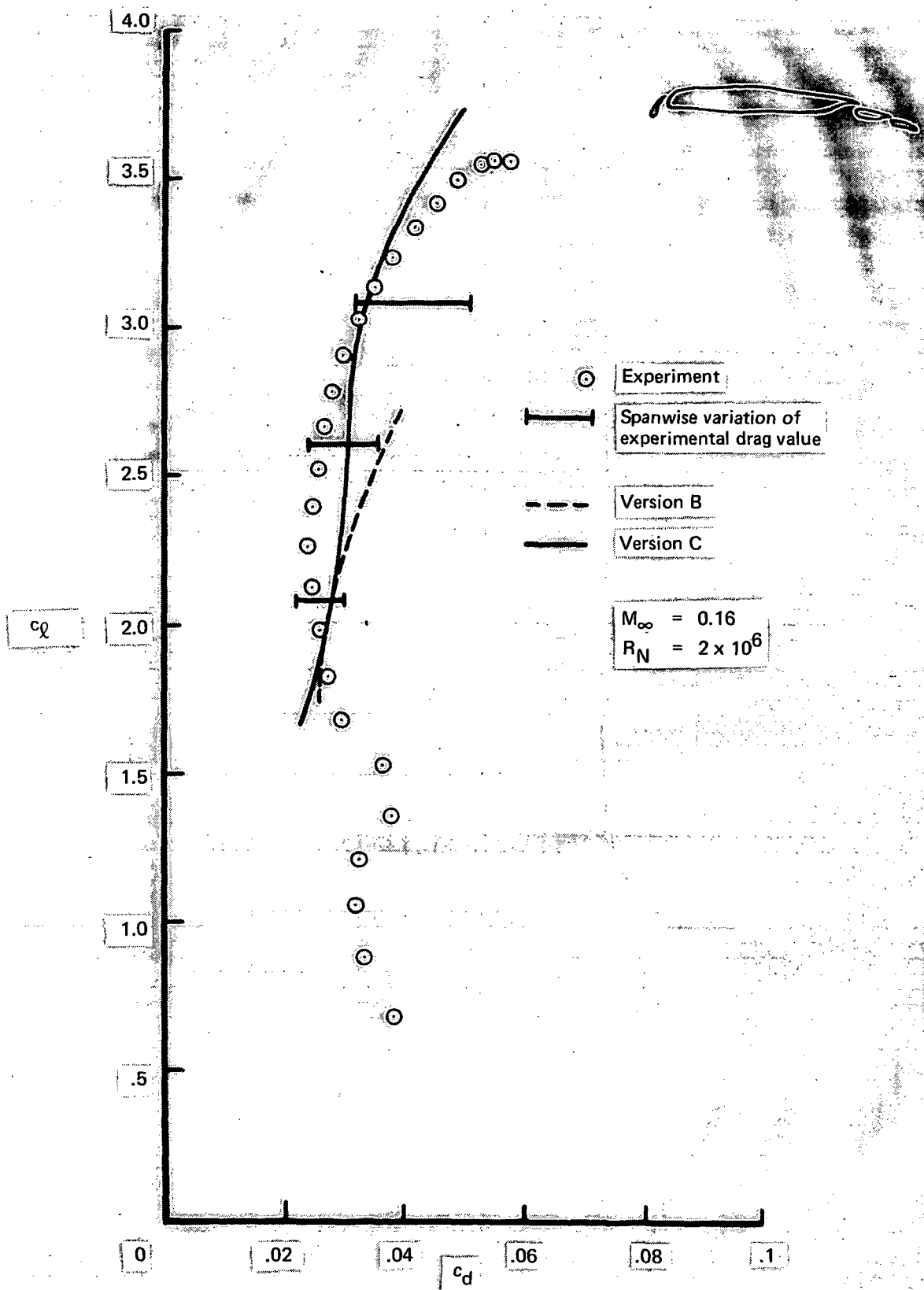


Figure 24. - Drag Polar of Boeing Four-Element Airfoil

supporting brackets and pressure taps. The maximum spanwise variation of the measured airfoil drag is shown in figure 24. The highest drag values were recorded downstream of the flap support brackets and the lowest downstream of the pressure taps.

All attempts failed when using the baseline version of the program and program Version A to obtain a converged solution for this airfoil. Program Version B arrived at converged solutions between  $8^\circ$  and  $20^\circ$  angle of attack, but underpredicted the lift by a considerable amount (fig. 23). The improvement of the predictions by Version C is remarkable. But the reader should note that the potential flow solution already provides a very good approximation to the lift curve. Program Version C overpredicts the lift at high angles of attack, which is expected since the program does not model flow separation. However, the program accurately indicates the onset of trailing edge stall at about  $16^\circ$  angle of attack, thereby warning the user that above this angle of attack it operates outside its range of validity.

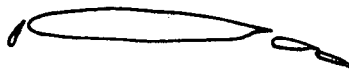
The theoretical values of the profile drag of Version C, (figs. 24 and 25), is relatively close to the measured profile drag. In judging the quality of the agreement of the two types of drag curves, the reader should recall the problems of two-dimensional high lift testing and the uncertainties in applying the Squire and Young formula to theoretical drag predictions.

Theoretical pitching moment characteristics are compared with experimental data in figure 26. The discrepancy of the curves at higher lift values is due to trailing edge stall that is not modeled by the program.

Figure 27 and table 4 demonstrate the excellent convergence characteristics of the new program Version C. Table 4 lists the updates of the position of the wake centerlines emanating from the trailing edge of each airfoil component during each cycle of the overall iteration procedure.

Figures 28 through 33 contain comparisons of theoretical and experimental surface pressures at  $8.4^\circ$  angle of attack. These figures confirm the earlier findings that Version C indeed provides the best theoretical results. Differences between the theory of Version C and experiment are noted in cove regions and on the second trailing edge flap (fig. 28, 32, and 33). Again, the need to model the flow in the cove region of airfoils is apparent. Other differences in the surface pressures are due to an insufficient number of surface points used in the discretization of the airfoil geometry. Figure 34 contains the number of surface points of each airfoil component. Numerical experience in aerodynamics has shown that at least 50 to 60 surface points are needed for an adequate representation of each airfoil component. The insufficient discretization of the Boeing high lift airfoil was dictated by the limitations of program Versions A and B to a total of 165 surface points. Program Version C used the same number of surface points to ensure a fair comparison of the program versions; but is not limited to such a small number of geometry points.

Figure 34 demonstrates the capability of Version C to compute smooth streamlines in the vicinity of airfoil surfaces.



⊙ Experiment

— Version C

$M_\infty = 0.16$

$R_N = 2 \times 10^6$

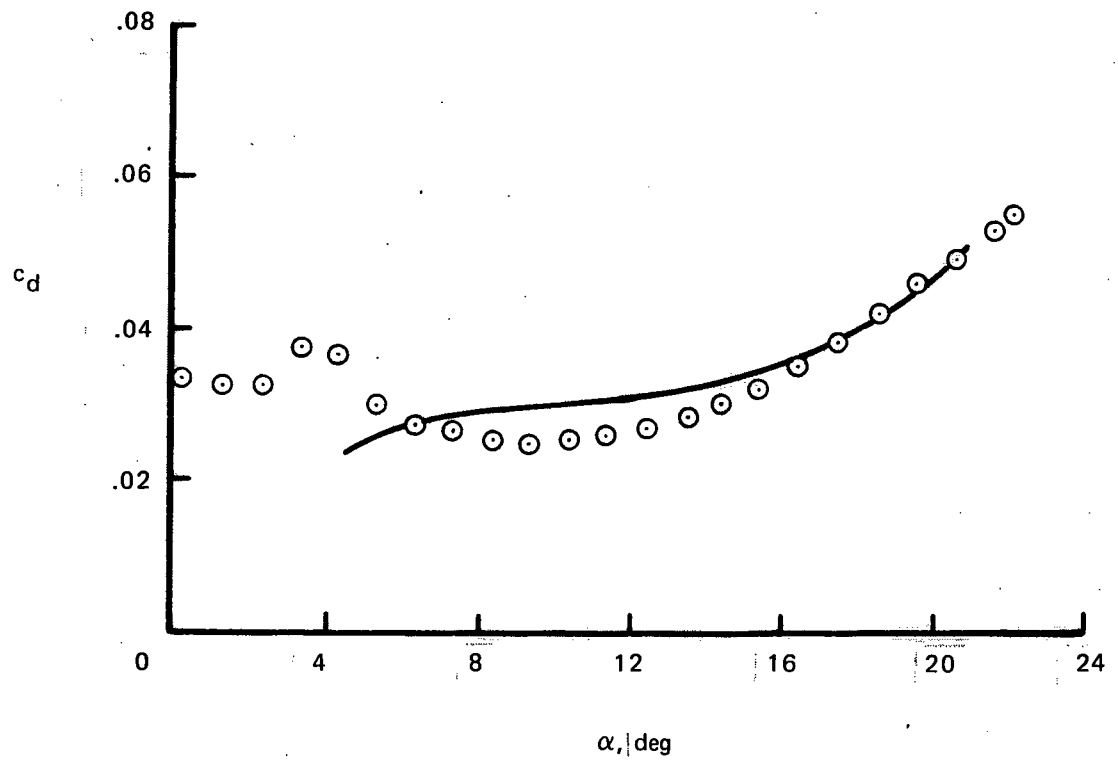


Figure 25. — Drag of Boeing Four-Element Airfoil

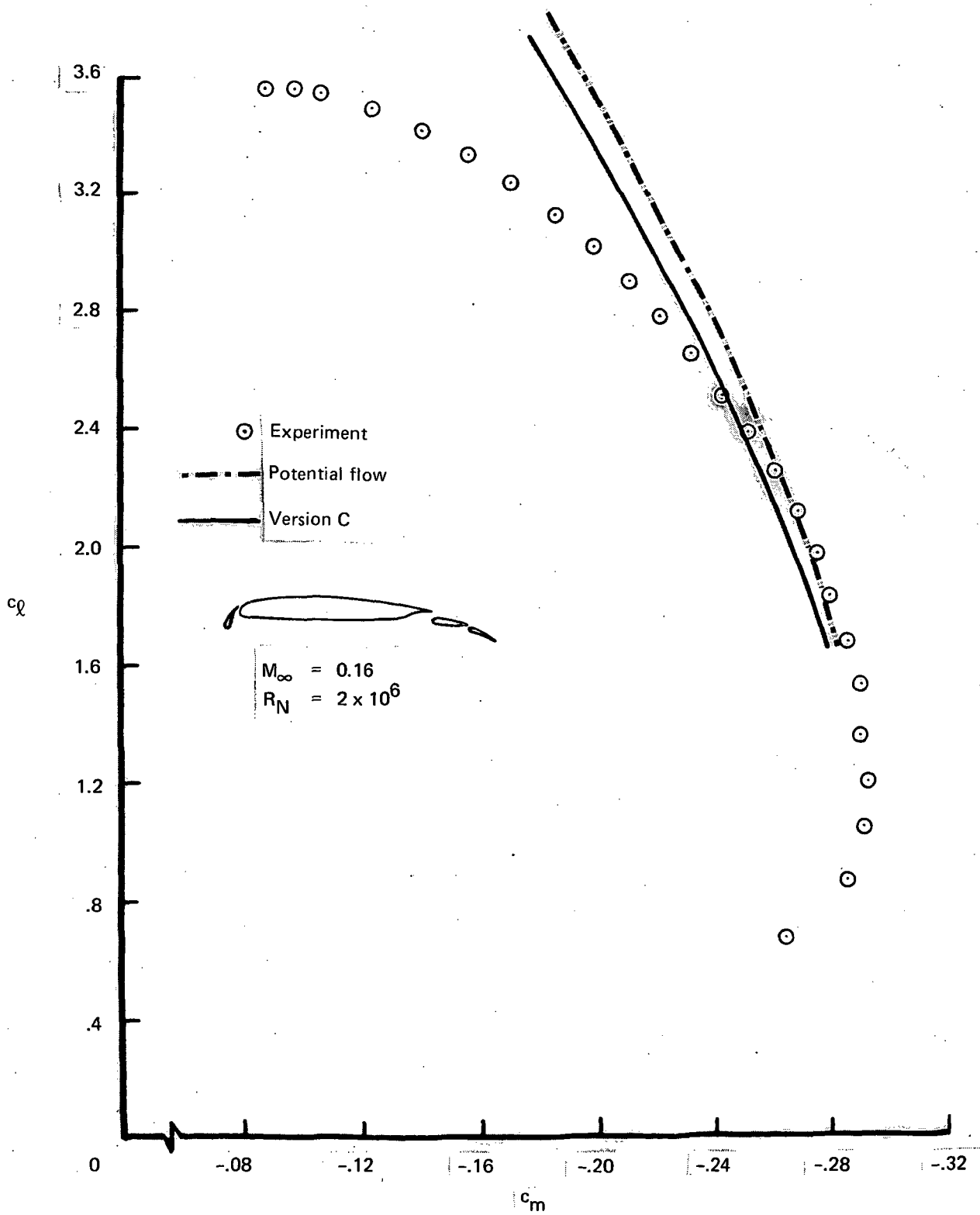


Figure 26. — Pitching Moment Characteristics of Boeing Four-Element Airfoil

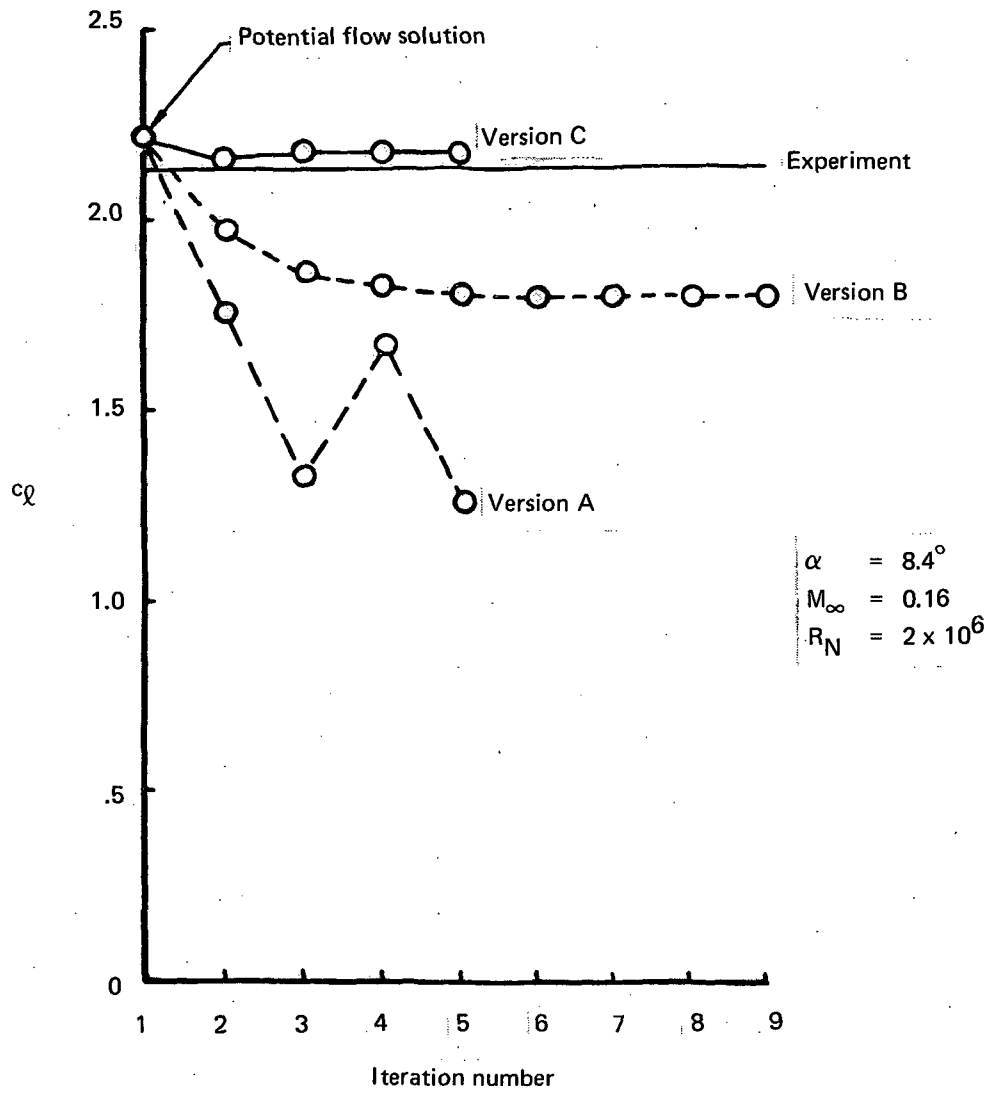
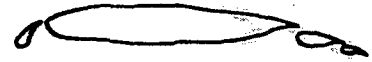


Figure 27. — Convergence Characteristics of Program Versions for Boeing Four-Element Airfoil

**Table 4. – Convergence Characteristics of Version C of  
NASA/Lockheed Program**

**Boeing Four-Element Airfoil**

$\alpha = 8.4^\circ$

$M_\infty = 0.16$

$R_N = 2 \times 10^6$

Iteration number	Lift	Wake centerline updates
1	2.211	2
2	2.158	1
3	2.176	1
4	2.175	0
5	2.173	0

$\alpha = 12.45^\circ$

$M_\infty = 0.16$

$R_N = 2 \times 10^6$

Iteration number	Lift	Wake centerline updates
1	2.748	1
2	2.676	1
3	2.698	1
4	2.701	1
5	2.699	1

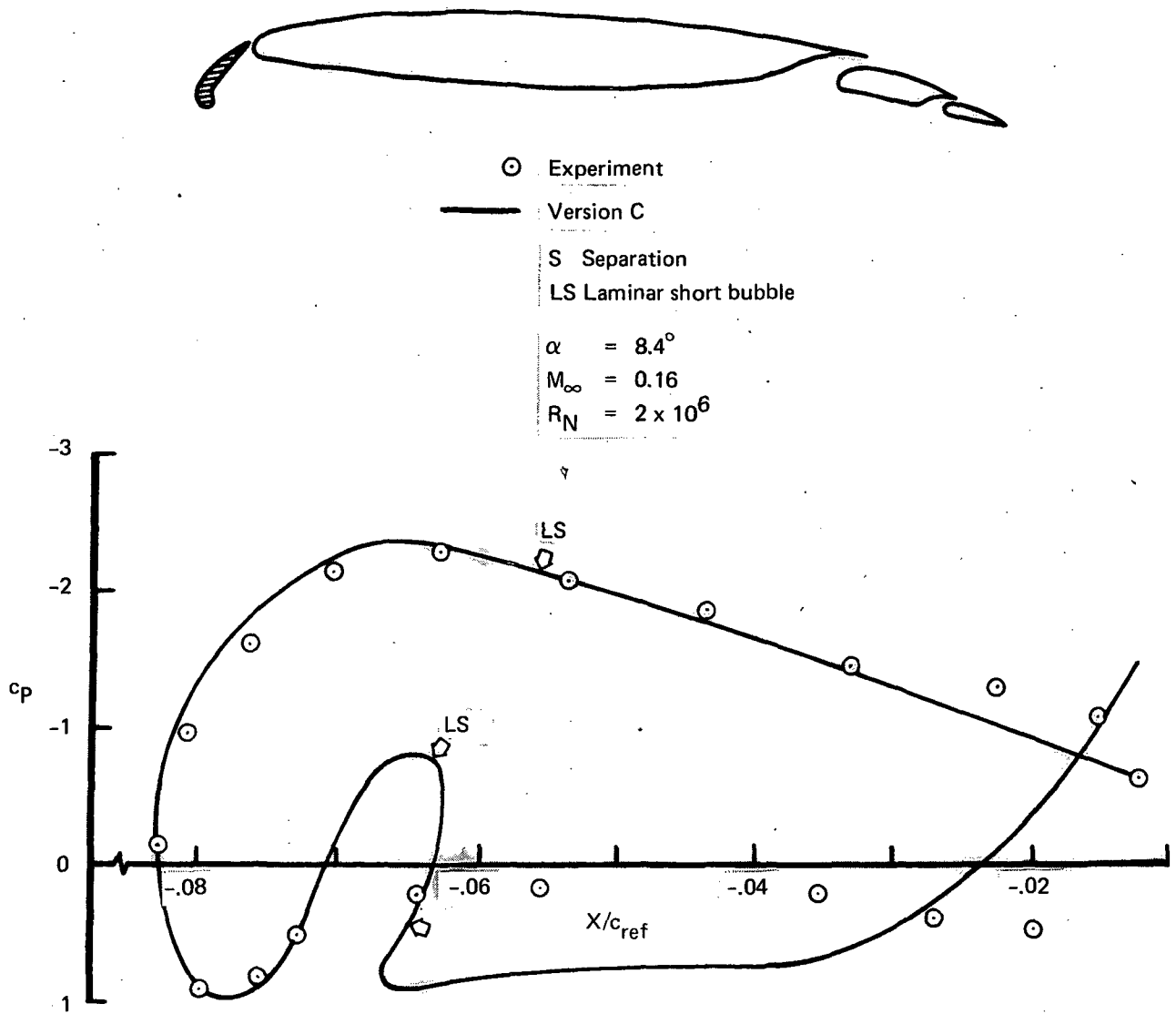


Figure 28. — Slat Surface Pressures of Boeing Four-Element Airfoil

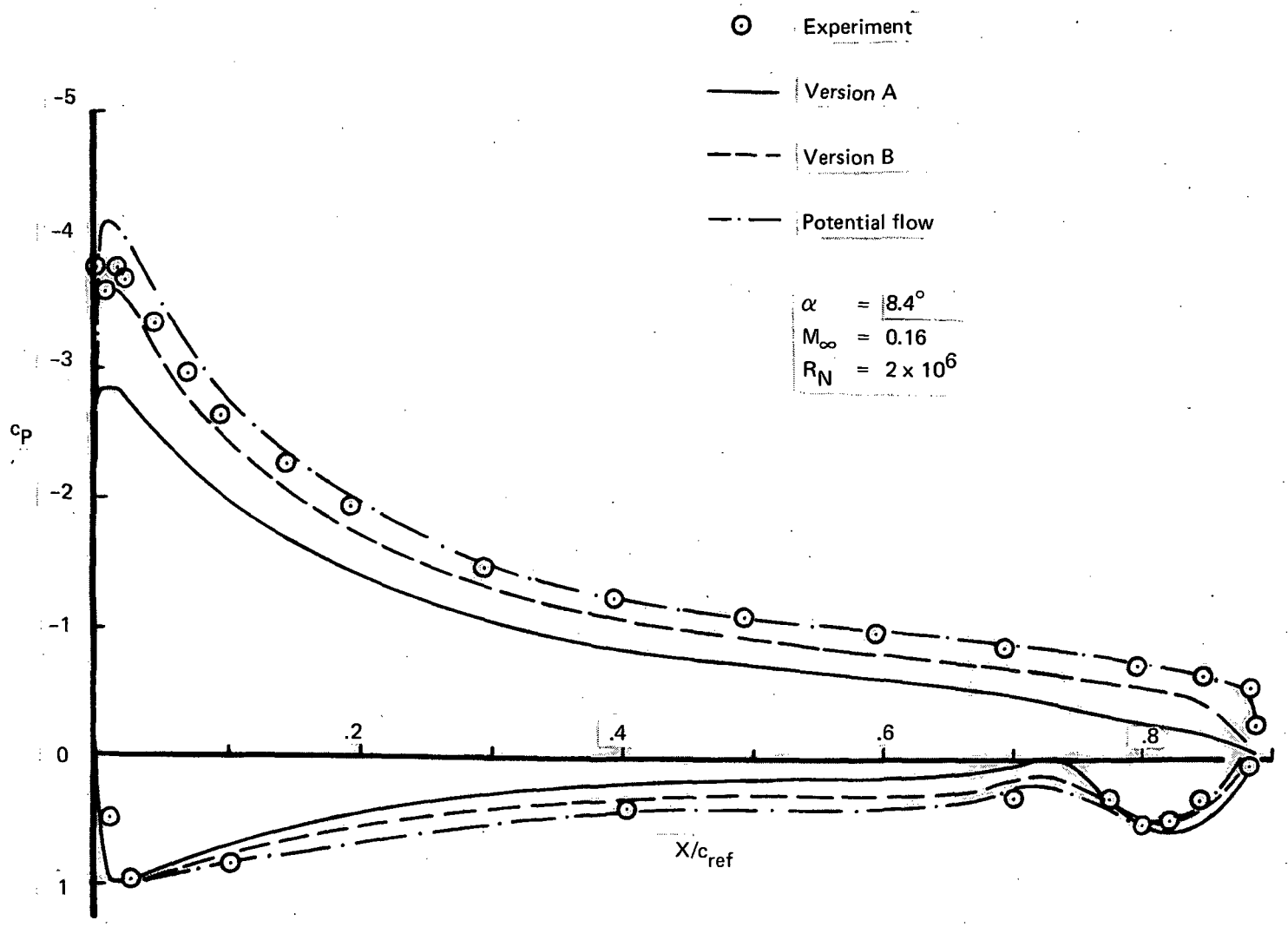


Figure 29. — Pressure Distribution Comparison for Main Wing Section of Boeing Four-Element High-Lift Airfoil

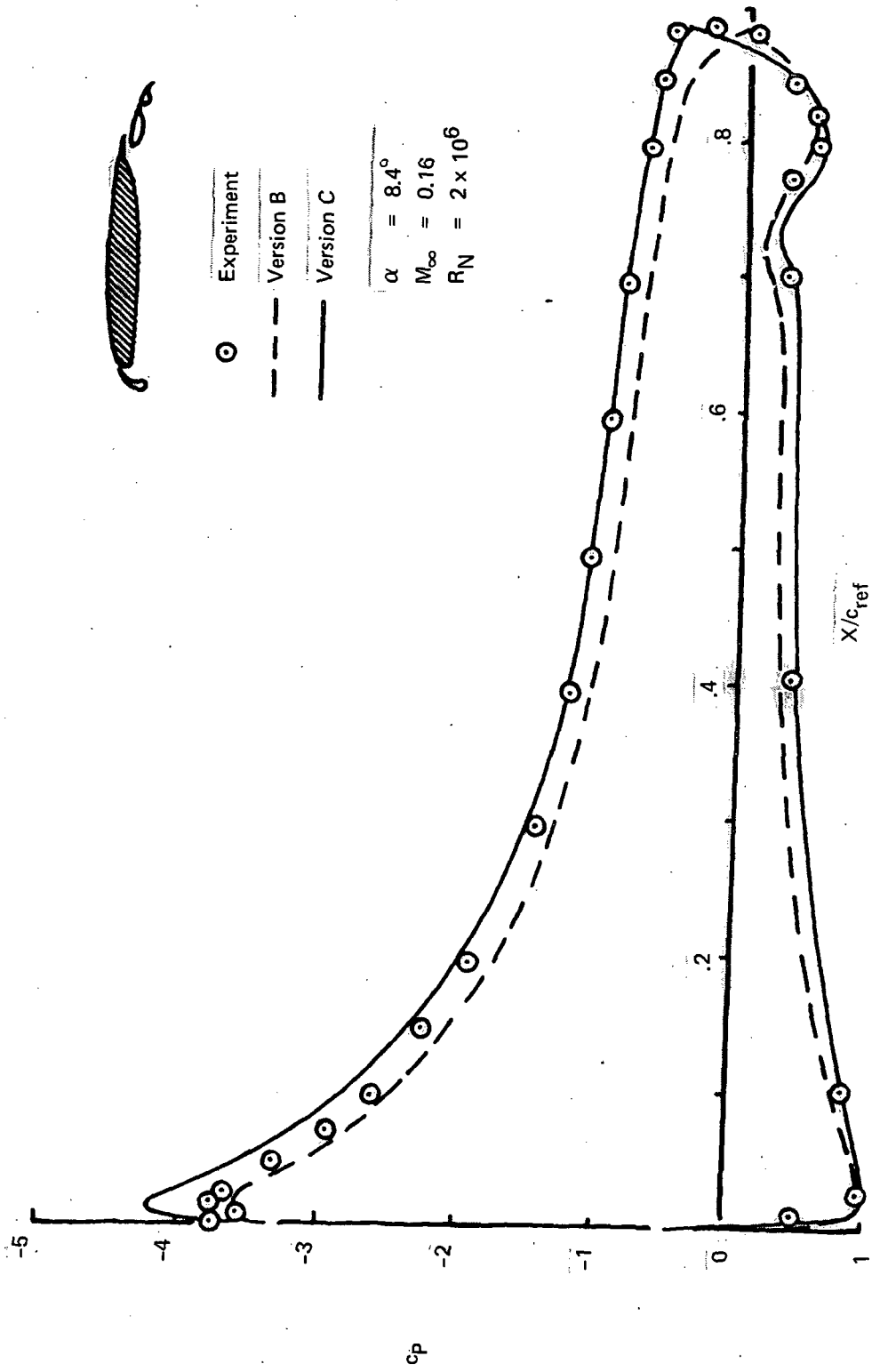


Figure 30. — Wing Surface Pressures of Boeing Four-Element Airfoil

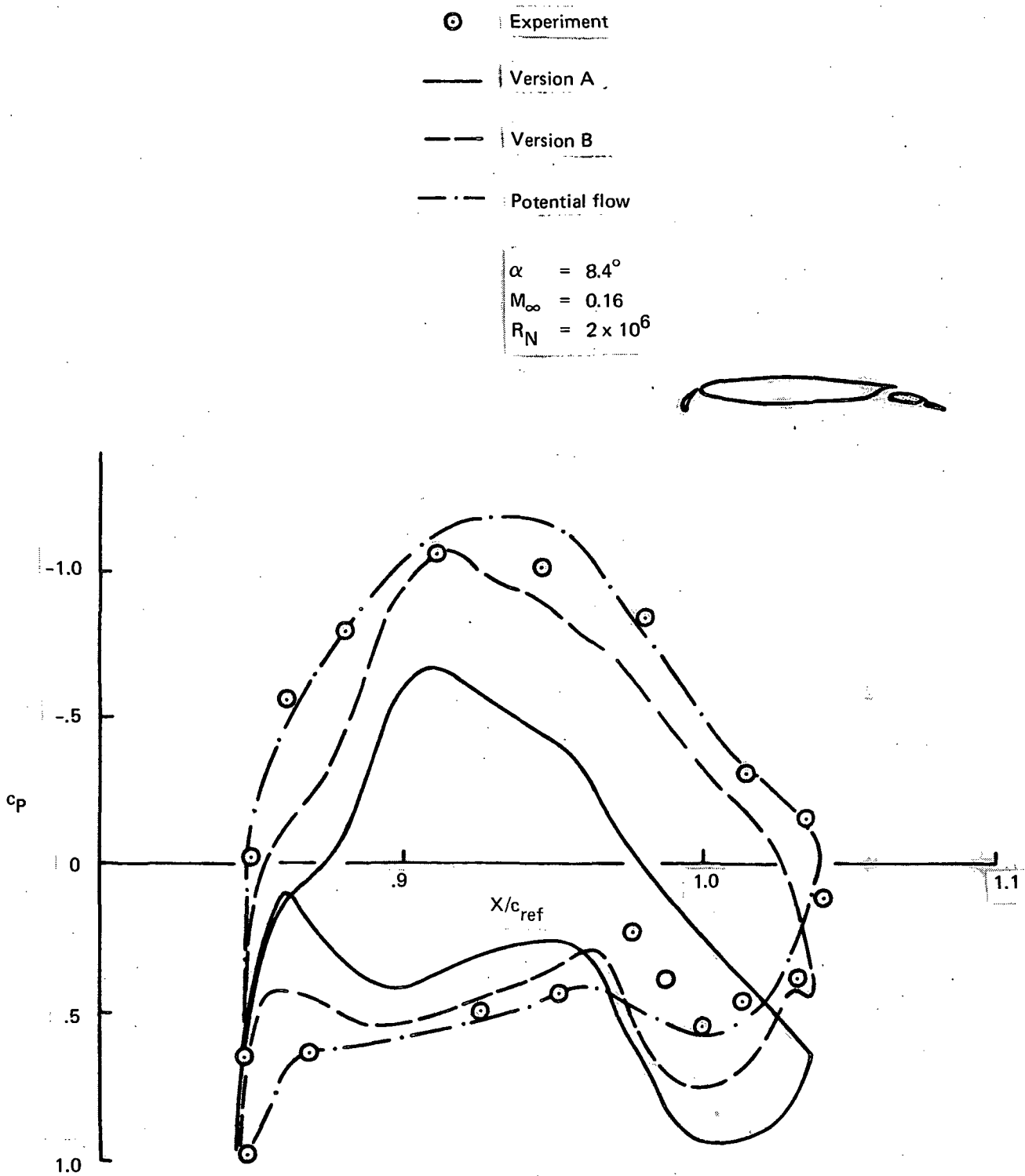


Figure 31. — Pressure Distribution Comparison for Main Flap of Boeing Four-Element High-Lift Airfoil

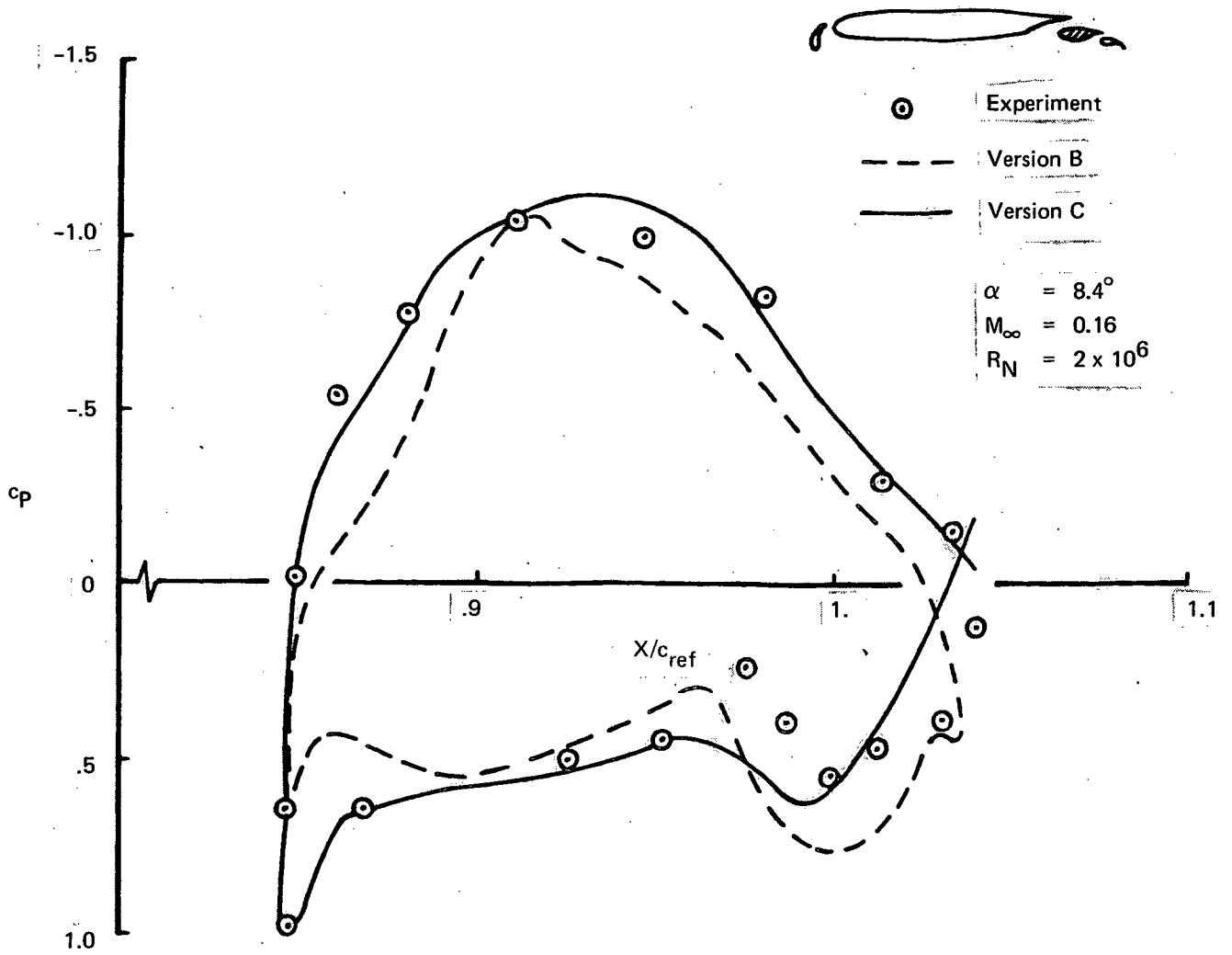


Figure 32. — Main Flap Surface Pressures of Boeing Four-Element Airfoil

○ Experiment  
 — Version C  
 S Separation  
 LS Laminar short bubble

$\alpha = 8.4^\circ$   
 $M_\infty = 0.16$   
 $R_N = 2 \times 10^6$

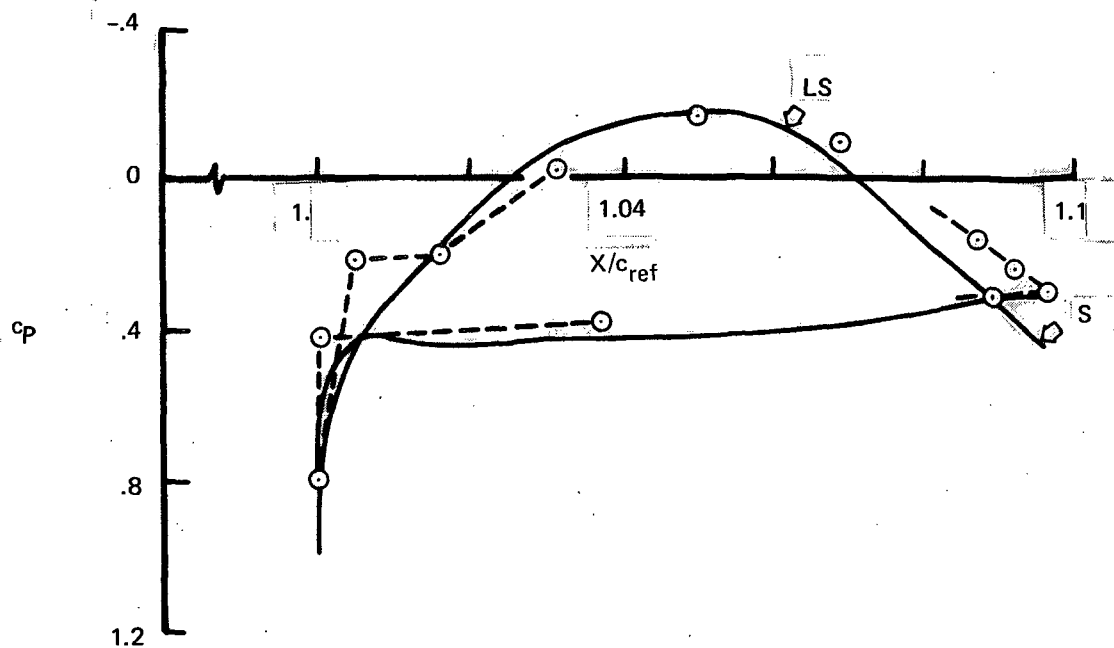


Figure 33. — Trailing-Edge Flap Pressures of Boeing Four-Element Airfoil

$\alpha = 8.4^\circ$   
 $M_\infty = 0.16$   
 $R_N = 2 \times 10^6$

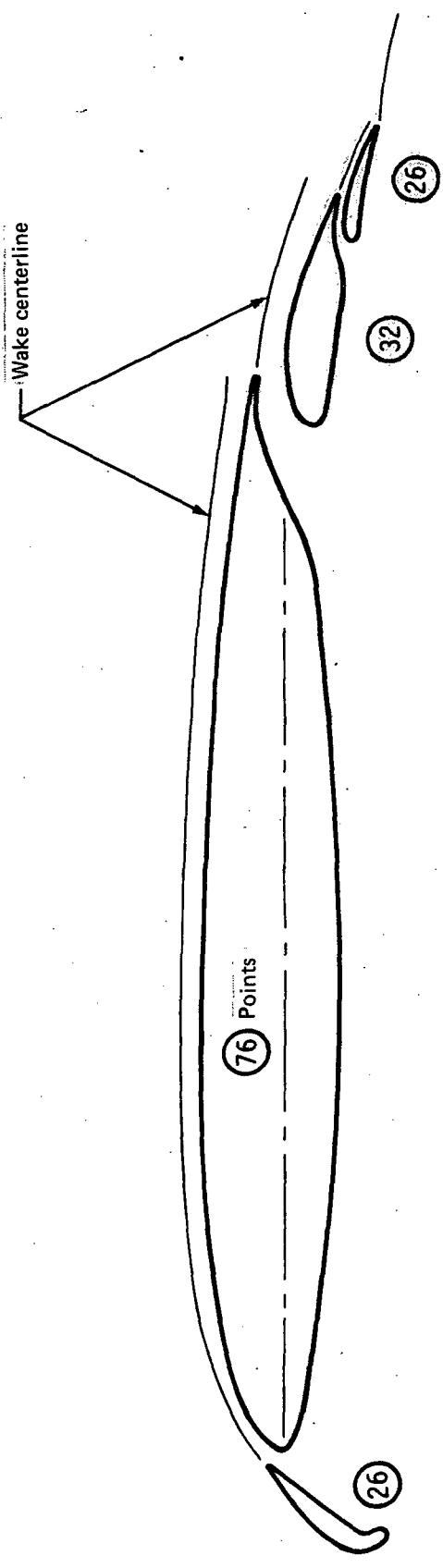


Figure 34. — Computed Position of Wake Centerlines of Boeing Four-Element Airfoil

Figure 35 through 39 compare predictions of boundary layer parameters, figure 38 deserves special attention. Boundary layer velocity profiles on the upper surface of the main component are shown at several chordwise stations. The experimental velocity profiles reveal that very little confluence of slat wake and wing boundary layer has taken place, and that an initially existing weak confluent boundary layer above the wing has degenerated early into an ordinary turbulent boundary layer. This feature of the flow field is very well simulated by Version C.

#### LJUNGSTRÖM'S AIRFOIL

Figure 40 shows lift and drag curves of the Ljungström four-element airfoil (ref. 16). Converged theoretical solutions were only obtained at  $\alpha = 10^\circ$  and  $16^\circ$  angle of attack. Obviously, successful theoretical predictions for this type of airfoil will require a model of cove separation.

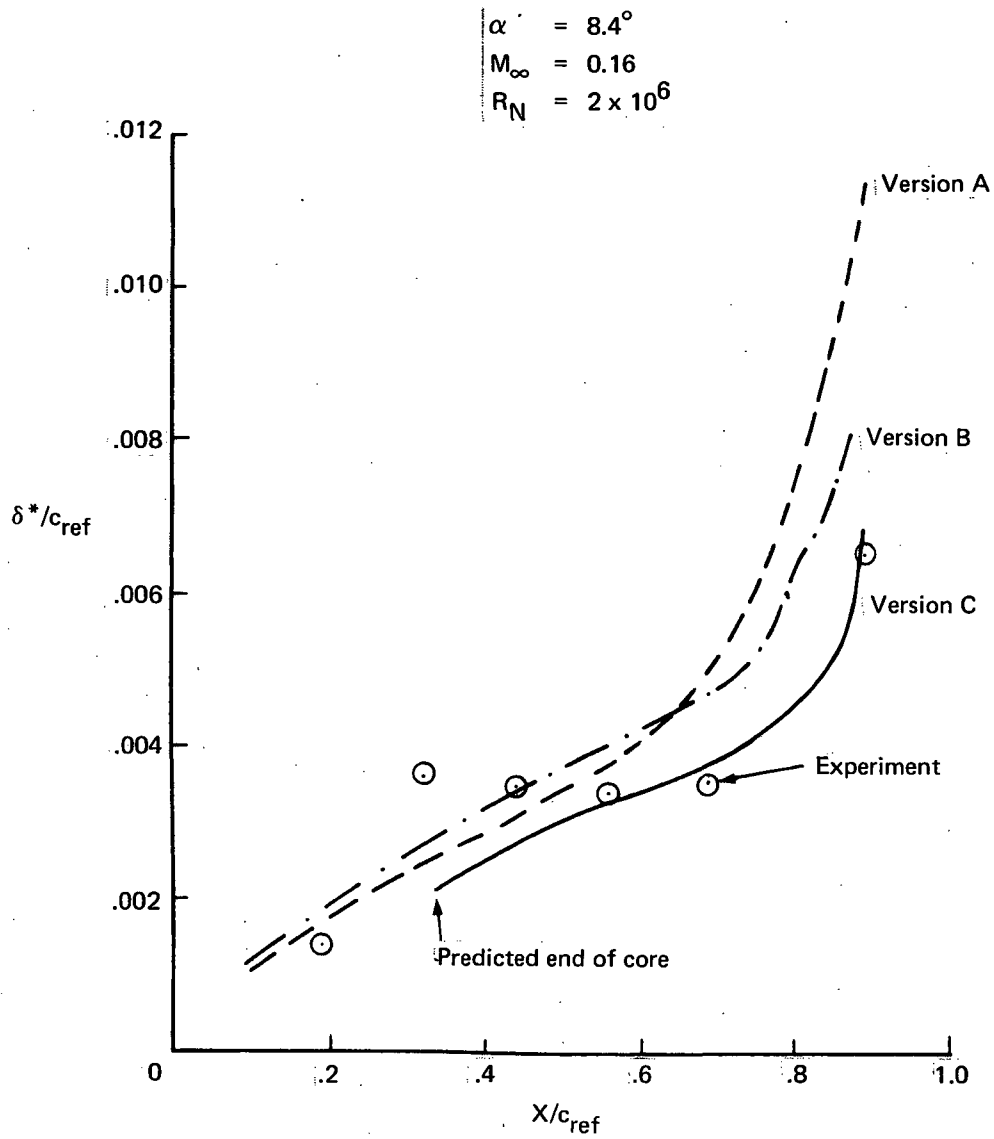


Figure 35. — Boundary Layer Displacement Thickness on Upper Surface of Main Wing of Boeing Four-Element Airfoil

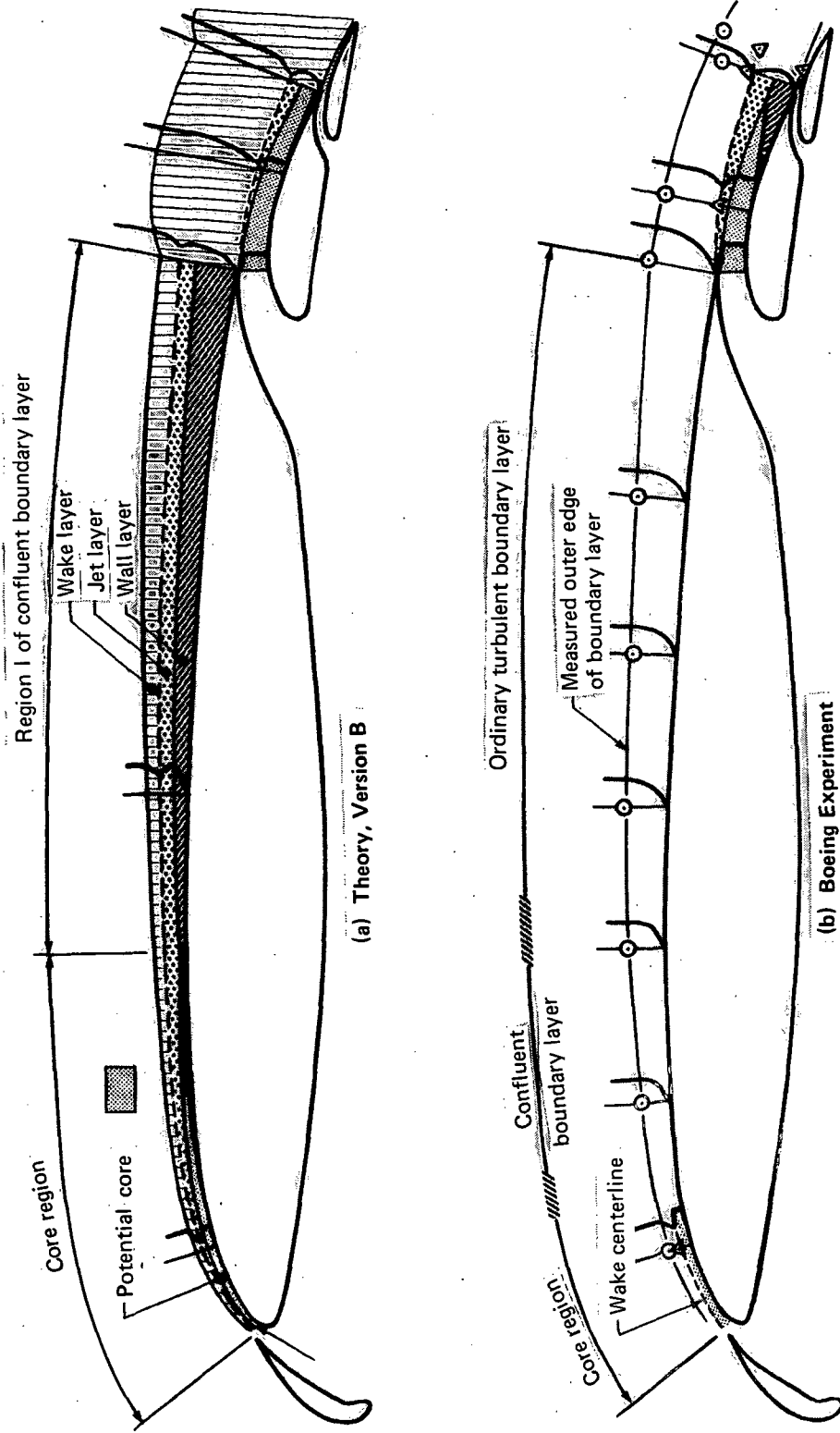


Figure 36. — Viscous Flow on Upper Surface of Boeing Four-Element High-Lift Airfoil —  $\alpha = 8.4^\circ$ ,  $M_\infty = 0.16$ ,  $R_N = 2 \times 10^6$

$\alpha = 8.4^\circ$   
 $M_\infty = 0.16$   
 $R_N = 2 \times 10^6$

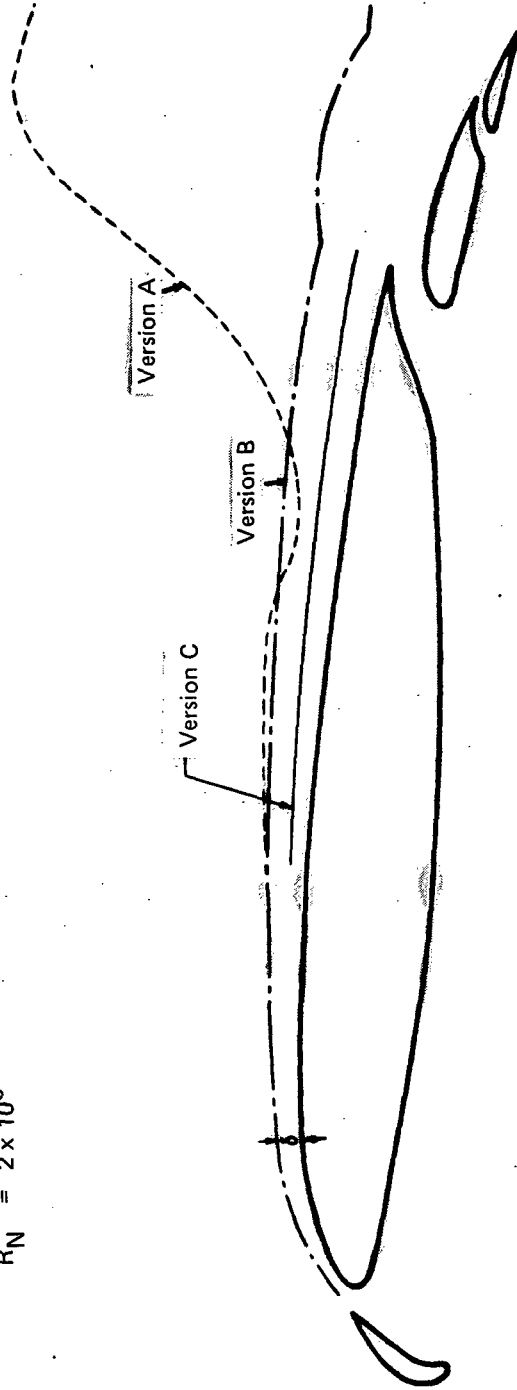


Figure 37. — Computed Boundary Layer Thickness on Upper Surface of Boeing Four-Element Airfoil

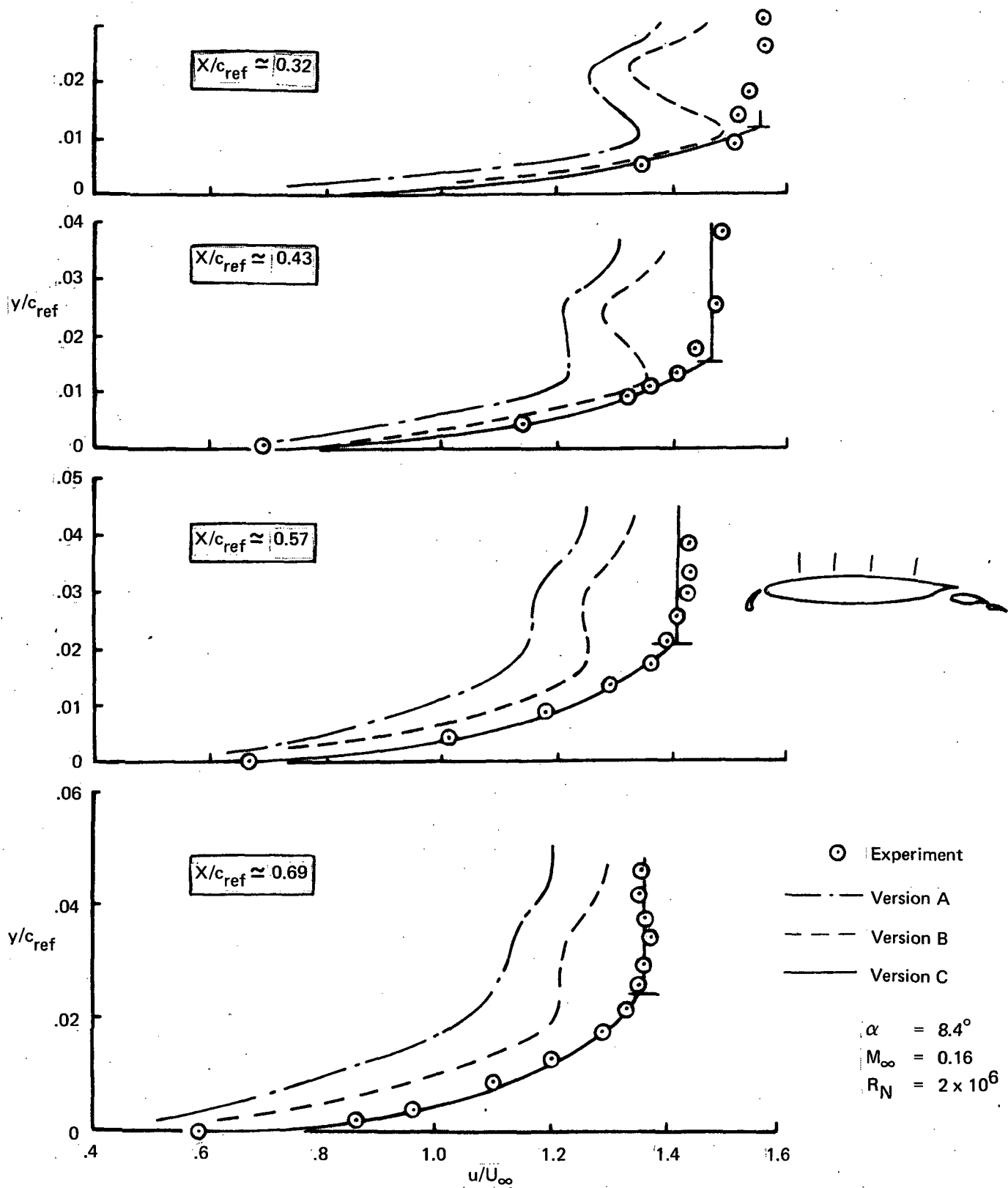


Figure 38. — Boundary Layer Profiles on Upper Wing Surface of Boeing Four-Element Airfoil

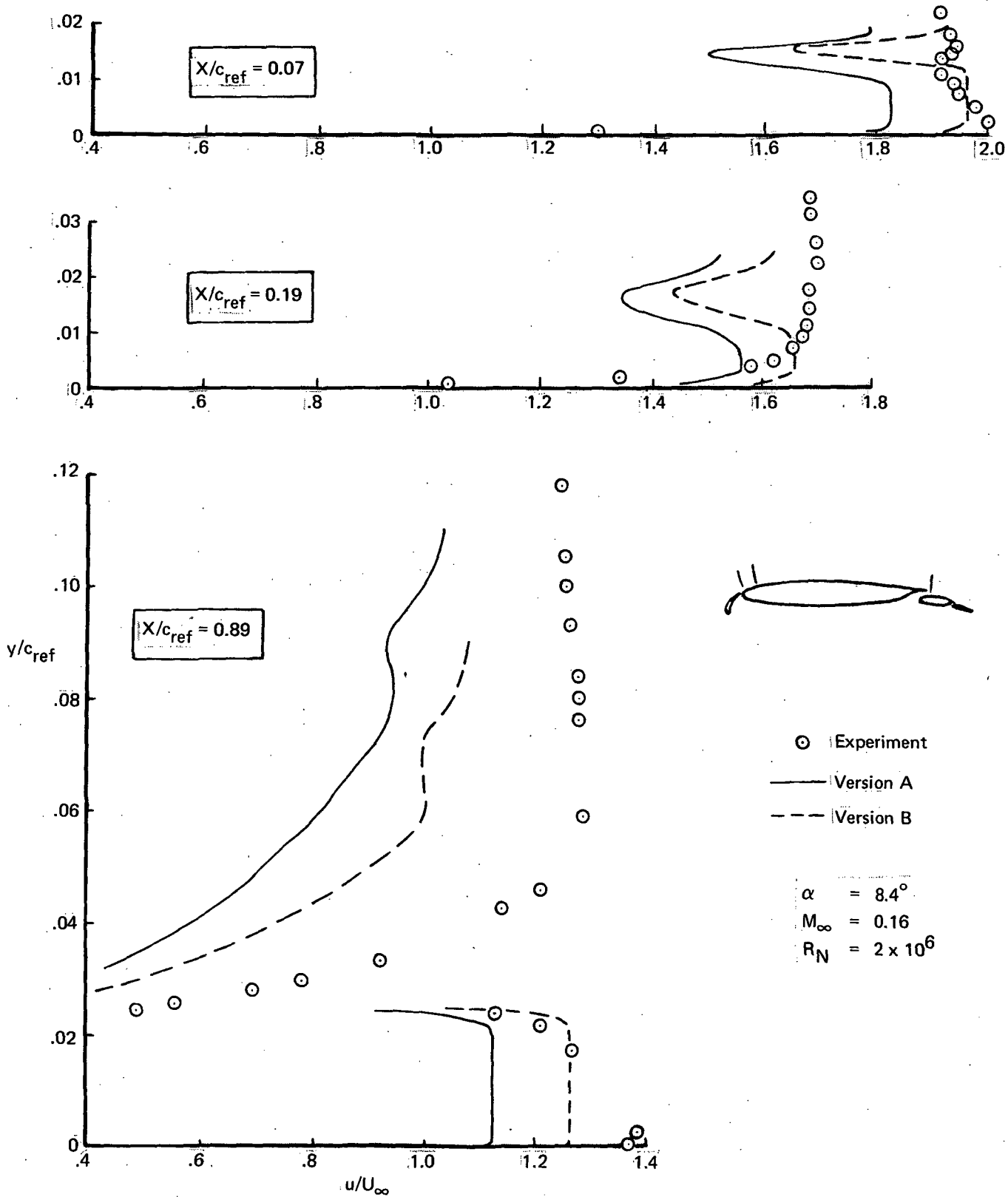


Figure 39. — Boundary Layer Profiles of Boeing Four-Element High-Lift Airfoil

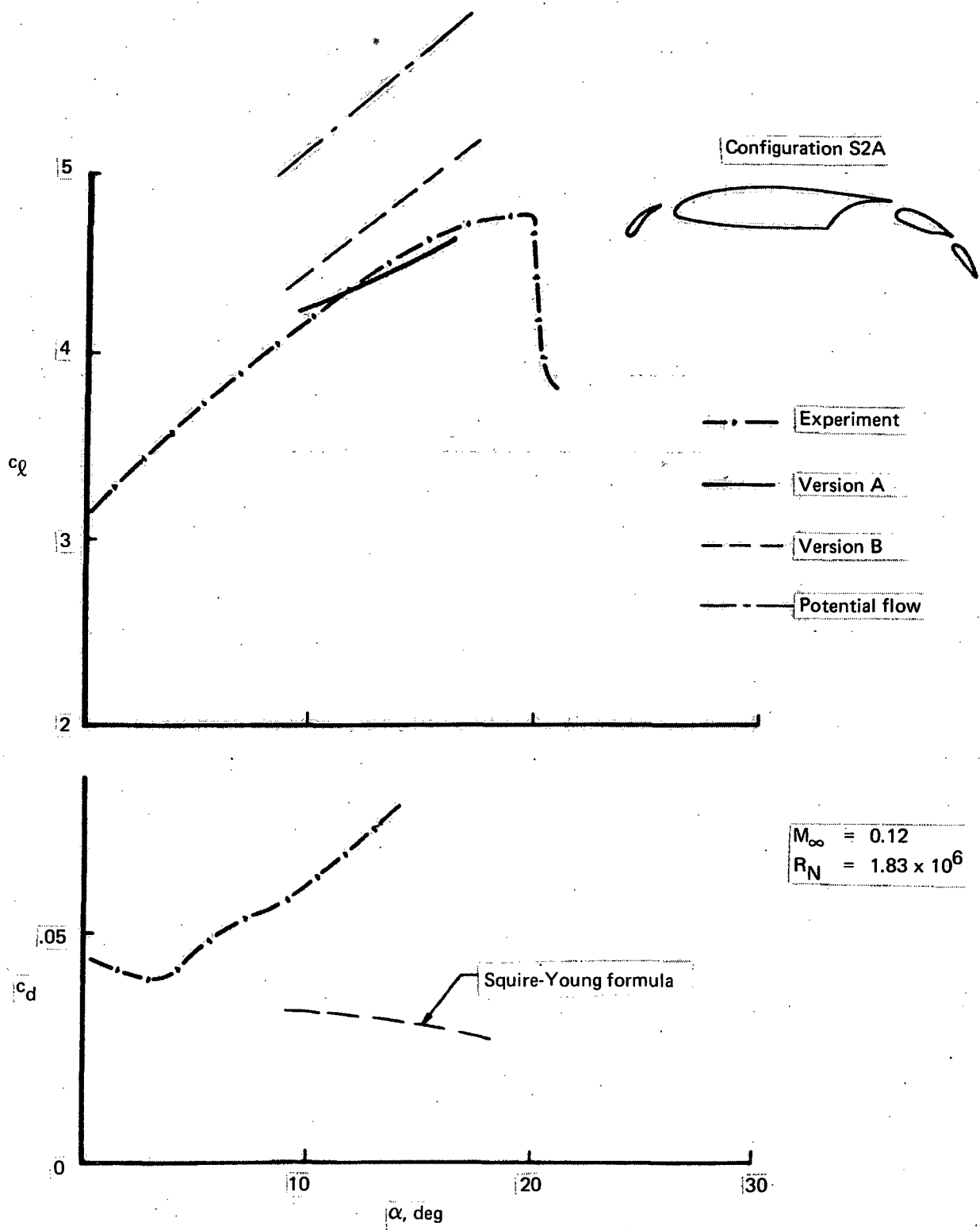


Figure 40. — Comparison of Lift- and Drag-Coefficient for Ljungström Four-Element Airfoil

## CONCLUSIONS

Several versions of the NASA-Lockheed computer program were evaluated on the basis of experimental high lift data that had not been available when the original version of the code was published. Based on a relatively short evaluation phase of a few months, the following conclusions about the reliability and quality of the theoretical predictions are drawn.

- Program Version C, developed by The Boeing Company, is the most reliable and accurate version. It produced converged solutions within a few iteration cycles for all test cases run, while the other program versions frequently failed to provide any result at all. The improvement of the accuracy of the program predictions is due to several modifications of the aerodynamic model; mainly due to a better representation of the boundary layer displacement effects, and an improved model of the potential core region.
- All program versions produced the best results in cases where most of the flow is attached to the airfoil's surface. This is consistent with the basic assumption of attached flow, but the range of applicability of the program should be extended by adding separation models for the cove region and for trailing edge stall.
- The usefulness of the confluent boundary layer method of Goradia and its modification utilizing Coles' velocity profile for the purpose of predicting the onset of confluent boundary layer separation, has yet to be tested. Optimized configurations were chosen for most of the program evaluation with little confluence of wakes and boundary layers.
- The performance of the program needs to be tested for configurations at off-design conditions.
- The evaluation of the computer program was hampered by the shortage of reliable experimental high lift data. Additional wind tunnel testing of some of the more important high lift airfoil configurations would increase the confidence in their performance predictions.

Boeing Commercial Airplane Company  
P.O. Box 3707  
Seattle, Washington 98124  
December, 1977

## REFERENCES

1. Stevens, W. A.; Goradia, S. H.; and Braden, J. A.: *Mathematical Model for Two-Dimensional Multi-Component Airfoils in Viscous Flows*. NASA CR-1843, July 1971.
2. Morgan, H. L., Jr.: "A Computer Program for the Analysis of Multi-Element Airfoils in Two-Dimensional Subsonic, Viscous Flow." Aerodynamic Analyses Requiring Advanced Computers Conference. Langley Research Center, Hampton, Virginia, March 1975.
3. Brune, G. W.; Hahn, M.; Mark, J. L.; and Manke, J. W.: *Modification and Clarification of the NASA/Lockheed Multi-Element Airfoil Computer Program*. Boeing document, D6-45072, February 1977.
4. Brune, G. W.; and Manke, J. W.: *An Improved Version of the NASA/Lockheed Multi-Element Airfoil Analysis Computer Program*. NASA CR-145323, March 1978.
5. Nash, J. R.; and Hicks, S. G.: *An Integral Method Including the Effects of Upstream History on the Turbulent Shear Stress*. Computation of Turbulent Boundary Layers - 1968. AFOSR-IFP-Stanford Conference, August 1968.
6. Squire, H. B.; and Young, B. A.: "The Calculation of the Profile Drag of Airfoils." R&M No. 1838, British A.R.C., November 1937.
7. Green, J. E.; Weeks, D. J.; and Brooman, J. W. F.: *Prediction of Turbulent Boundary Layers and Wakes in Compressible Flow by a Lag-Entrainment Method*. RAE TR 72231, January 1973.
8. Coles, D. E.: "The Law of the Wake in the Turbulent Boundary Layer." *J. of Fluid Mech.*, vol. I, pp. 191-226, 1956.
9. McGhee, R. J.; and Beasley, W. D.: *Low Speed Aerodynamic Characteristics of a 17-Percent Thick Airfoil Section Designed for General Aviation Applications*. NASA TN D-7428, 1973.
10. NASA-Langley: *Conference on Free Turbulent Shear Flows*. NASA SP-321, July 1972.
11. Chevray, R.; and Kovasznay, L. S. G.: "Turbulent Measurements in the Wake of a Thin Flat Plate." *AIAA J.*, vol. 7, no. 8, pp. 1641-1643, August 1969.
12. Wentz, W. H. Jr.; and Seetharam, H. C.: *Development of a Fowler Flap System for a High Performance General Aviation Airfoil*. NASA CR-2443, December 1974.

13. Wentz, W. H. Jr.; Seetharam, H. C.; and Fisco, K. A.: *Force and Pressure Tests of the GA(W)-1 Airfoil With a 20% Aileron and Pressure Tests With a 30% Fowler Flap.* NASA CR-2833, June 1977.
14. Seetharam, H. C.; and Wentz, W. H., Jr.: *A Low Speed Two-Dimensional Study of Flow Separation on the GA(W)-1 Airfoil With 30-Percent Chord Fowler Flap.* NASA CR-2844, May 1977.
15. Foster, D. N.; Irwin, H. P. A. H.; and Williams, B. R.: "The Two-Dimensional Flow Around a Slotted Flap." *R&M No. 3681, British A.R.C.*, 1971.
16. Ljungström, B. L. G.: "Two-Dimensional Wind Tunnel Experiments With Single and Double Slotted Flaps." *FFA TN AU-1083, October 1975.*